J. Fluid Mech. (2017), *vol.* 828, *pp.* 135–174. © Cambridge University Press 2017
doi:10.1017/jfm.2017.505

Acoustics of permeo-elastic materials

Rodolfo Venegas[1],† **and Claude Boutin**[1]

[1]Université de Lyon - Ecole Nationale des Travaux Publics de l'Etat - LGCB/LTDS - UMR-CNRS 5513, Rue Maurice Audin, 69518 Vaulx-en-Velin, France

(Received 19 January 2017; revised 11 May 2017; accepted 19 July 2017; first published online 31 August 2017)

In the dynamics of Biot poroelastic materials, the fluid flow is not affected by the deformation of the solid elastic frame. In contrast, in permeable materials whose solid stiff frames have flexible thin flat films attached, i.e. permeo-elastic materials, the fluid flow can be significantly modified by the presence of the films. As a consequence of the local fluid–film interaction, and in particular of the local resonances, the classical local physics is changed and departs from that leading to the Biot description. In this paper, the two-scale asymptotic homogenisation method is used to derive the macroscopic description of sound propagation in air-saturated permeo-elastic materials. This description is asymptotically analysed to determine the conditions for which the geometrical and mechanical properties of the films strongly affect the effective properties of the material. The developed theory is illustrated numerically and validated experimentally for a prototype material, evidencing the atypical acoustic behaviour.

Key words: acoustics, viscoelasticity, wave–structure interactions

1. Introduction

This paper investigates mass transport and acoustic wave propagation in permeo-elastic materials. This type of material is characterised by (i) a connected pore network saturated with a Newtonian fluid and (ii) a solid frame made of a stiff skeleton onto which highly flexible thin films are fixed. In contrast to Biot poroelastic materials (Biot 1956*a*,*b*), where the fluid flow is not affected by the deformation of the solid frame, a fluid–film interaction is present in permeo-elastic materials. This induces significant modifications of the physics determining the mass transport of the fluid through the porous material. Consequently, the concept of permeability in the permanent or dynamic regime should be revisited. Specifically, it will be shown in this paper that the constitutive fluid flow law accounts for the elastic and kinematic energy of the films in addition to the conventional viscous dissipation and inertia of the fluid. As a consequence, unconventional flow regimes exist where the fluid–film system behaves as an equivalent visco-elastic fluid and local fluid–film resonances can be observed in specific frequency ranges. Accordingly, the acoustic behaviour departs from the standard poro-acoustic macroscopic description (Biot 1956*a*,*b*; Auriault, Borne & Chambon 1985; Lafarge *et al.* 1997).

† Email address for correspondence: rodolfogustavo.venegascastillo@entpe.fr

Modelling of the overall effect of the multiple fluid–structure interactions that occur in permeo-elastic media is a challenging and computationally demanding task. In addition, direct simulation of the fluid flow is practically out of reach due to the multiscale nature of the problem. For these reasons, an effective model of such media is established in this paper by using an upscaling approach based on the two-scale asymptotic homogenisation method (Sanchez-Palencia 1980; Auriault, Boutin & Geindreau 2009). Potential applications of the theory developed in this work include, for example, the design of novel materials with unconventional tunable properties in acoustic engineering (Boutin, Royer & Auriault 1998; Bongard, Lissek & Mosig 2010; Krynkin *et al.* 2010; Venegas & Umnova 2011; Boutin 2013; Lafarge & Nemati 2013; Groby *et al.* 2015; Leclaire *et al.* 2015; Venegas & Boutin 2017), inverse methods in the mechanics of soft films (Leroy & Charlaix 2011) or the analysis of fluid flow in the presence of deformable membranes, e.g. bio-films or cell walls, in biomechanics (Dailey, Yalcin & Ghadiali 2007; Rubenstein, Yin & Frame 2015).

Fluid–structure interaction has been widely studied as a phenomenon playing a determining role in fluid mechanics, aeronautics, structural dynamics and biomechanics. In acoustics, for example, the fluid–structure interaction is mostly studied for large-scale vibro-acoustic applications (see Habault 1999) which commonly involve a single structural element interacting with the fluid. These developments are applied most commonly to shells or plates which may be impervious or perforated (Lee, Lee & Ng 2005; Bravo, Maudry & Pinhède 2012; Bolton 2013; Li, Cazzolato & Zander 2016) but also to other types of resonating elements such as Helmholtz resonators with elastic walls (Norris & Wickham 1993).

Considering the fluid interaction with multiple deformable solid elements, one may mention the studies of sound transmission in periodic arrays of shells (Krynkin *et al.* 2010) and sound absorption of packings of elastic hollow grains (Griffiths, Nennig & Job 2017). In addition, features of the acoustic wave propagation in the presence of a periodic array of elastic membranes have been investigated recently. For instance, an array of mass-loaded membranes and a tube periodically loaded with membranes transversely connected to open channels were investigated by Yang *et al.* (2008) and Bongard *et al.* (2010) respectively. Furthermore, a similar geometry was considered in Bolton (2013) to model sound propagation in macro-cellular polyolefin foams. In all of these cases, the effect of fluid–structure resonances is evidenced.

However, distributed fluid–structure interactions taking place at the pore scale within a porous medium have been rarely studied. This is because, in most practical cases, the stiffness of the solid frame is sufficiently large to withstand the pressure and drag force induced by the fluid flow which causes only a negligible deformation. Hence, the fluid flows as if the pore structure were perfectly rigid. This assumption has nevertheless been questioned in several works devoted to flow in porous media involving interaction with the solid frame in large deformation. These studies have been developed in statics and usually lead to nonlinear constitutive laws. In this context, for example, Lee & Mei (1997) investigated the validity of the Biot model and proposed a nonlinear Biot model for the case of non-symmetric cells. The analysis presented in Brown, Popov & Efendiev (2011) accounts for the evolution of the pore structure at a time scale much longer than that of the fluid flow. This leads to an evolutionary flow problem that is ruled by a classical tangent Darcy's law at each time. Therefore, the fluid–structure interaction acts only on the long time scale. In the paper by Brown, Popov & Efendiev (2014), a nonlinear Biot model that includes pore-scale deformation in the effective description was derived. Consequently,

the local cell problems are coupled to the macroscopic equations via the effective coefficients.

The present study differs from the above cited works because (i) only the deformable films, and not the whole solid, participate in the fluid–structure interaction and (ii) the pore fluid network is connected, i.e. the films do not close the pores. Owing to the additional assumptions of flow at low Reynolds number and of small deformation of the clamped elastic films, the derived macroscopic description is linear and accounts for the fluid–film interaction. In addition, it will be shown that the macroscopic mass balance remains unchanged, while the fluid flow constitutive law is modified. This is the opposite case to non-conventional porous media, where inner mechanisms induce local mass source terms that alter the mass balance without modifying the fluid flow constitutive law and its associated effective parameter (Boutin *et al.* 1998; Olny & Boutin 2003; Venegas & Umnova 2011; Boutin 2013; Leclaire *et al.* 2015; Venegas & Boutin 2017).

The structure of this paper is as follows. Section 2 is devoted to the modelling of permeo-elastic materials saturated with a Newtonian gas using the two-scale asymptotic homogenisation method (Sanchez-Palencia 1980; Auriault *et al.* 2009). Section 3 deals with the analysis of the effective properties, by which the macroscopic consequence of the fluid–film interaction at the pore scale is highlighted. It is shown that, in addition to the characteristic visco-inertial Biot frequency, the acoustic behaviour also depends on a characteristic visco-elastic frequency and two characteristic elasto-inertial frequencies. Furthermore, the limiting behaviour of the materials is presented with reference to the estimated characteristic frequencies. We investigate in § 4 the different possible fluid flow regimes and how the effective properties of the material behave in them. This allows us to identify the conditions for which the material geometry, the mechanical properties of the films and the physical properties of the saturating gas strongly affect the propagation of sound waves in the material. Also in this section, we present experimental data measured on a prototype material that evidences some of the non-conventional features theoretically predicted. The measured data are compared with numerical simulations, showing a reasonable agreement. The main findings are summarised in the conclusions.

2. Permeo-elastic materials

2.1. *Geometry description*

We consider a periodic permeable material whose fluid network is connected and saturated with a Newtonian fluid. Its frame is made of a very stiff skeleton onto which highly flexible thin flat films are fixed, as illustrated by figure 1. The characteristic length associated with the pores (or the period of the microstructure) is denoted as l. We consider relatively simple pore geometries for which a single characteristic size determines the fluid flow, i.e. no extreme geometrical contrasts in the pore space are considered. The volumes of the fluid network, the stiff solid and the representative elementary volume (REV) are Ω_f, Ω_s and Ω respectively. The surface of the stiff solid is denoted as Γ_s.

On the other hand, it is assumed that the in-plane dimension of the films, h, is of the same order of magnitude as the period of the microstructure, i.e. $h = O(l)$, while their thickness, t, is much smaller than the in-plane dimension, i.e. $t \ll h$. Therefore, the volume of the films can be neglected and the porosity of the material is calculated as $\phi = \Omega_f/\Omega$. Moreover, the films are made of an isotropic elastic material. These hypotheses allow us to model the films as Love–Kirchhoff plates (Love 1888) with

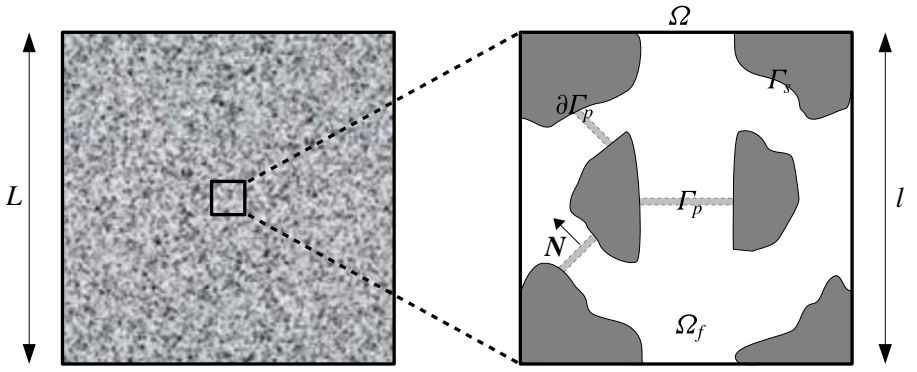

FIGURE 1. Diagram of the scales of a permeo-elastic material. The thin films are clamped to the stiff solid frame and the pore fluid network is connected.

negligible thickness and surface Γ_p whose behaviour is characterised by their out-of-plane 2D bending. The edges of the films, $\partial\Gamma_p$, are clamped to the stiff solid frame. This assumption can be (i) relaxed to consider other boundary conditions such as a combination of a free condition on some parts of $\partial\Gamma_p$ and a clamped condition on other parts of $\partial\Gamma_p$ or (ii) modified by considering membranes in tension instead of plates.

We are interested in long-wavelength sound propagation in permeo-elastic media. The macroscopic characteristic length L is related to the wavelength λ through $L = |\lambda|/2\pi$, and the disparity in length scales between the macroscopic and microscopic characteristic sizes provides the small parameter $\varepsilon = l/L \ll 1$.

2.2. *Governing equations at the local scale*

The equations that describe the propagation of harmonic sound waves ($\mathrm{e}^{\mathrm{i}\omega t}$) in rigid-frame porous materials are now recalled. These correspond to the linearised equations of conservation of momentum (2.1) and mass (2.2) along with the no-slip (2.3) boundary condition (Biot 1956*a*,*b*; Auriault *et al.* 1985, 2009). It should be noted that, for the sake of clarity in the presentation, adiabatic sound propagation is considered. However, the inclusion of thermal exchanges into the formulation is straightforward, as it will be shown below.

$$\mathrm{div}(\boldsymbol{\sigma}_f) = \mathrm{i}\omega\rho_0\boldsymbol{v} \quad \text{in } \Omega_f, \qquad \boldsymbol{\sigma}_f = 2\eta\boldsymbol{D}(\boldsymbol{v}) - p\boldsymbol{I}, \tag{2.1}$$

$$\mathrm{i}\omega\frac{p}{\gamma P_0} + \boldsymbol{\nabla}\cdot\boldsymbol{v} = 0 \quad \text{in } \Omega_f, \tag{2.2}$$

$$\boldsymbol{v} = \boldsymbol{0} \quad \text{on } \Gamma_s. \tag{2.3}$$

Here, $\boldsymbol{\sigma}_f$ is the fluid stress tensor, η is the dynamic viscosity, γ is the adiabatic exponent, $\boldsymbol{D}(\boldsymbol{v})$ is the strain rate tensor (defined through $2\boldsymbol{D}(\boldsymbol{v}) = \mathrm{grad}(\boldsymbol{v}) + (\mathrm{grad}(\boldsymbol{v}))^{\mathrm{T}}$), $\boldsymbol{v}$ is the fluid velocity, p is the pressure and $\boldsymbol{I}$ is the second-rank unitary tensor. The subscript 0 is used to denote equilibrium quantities.

The Love–Kirchhoff (in-vacuum) plate equations (Love 1888) are now recalled. The scalar out-of-plane displacement of the films, u, is governed by the equations

of equilibrium of transverse forces (2.4), moment balance (2.5) and the constitutive law (2.6):

$$\boldsymbol{\nabla}_p \cdot \boldsymbol{T} = -\rho_p t\omega^2 u \quad \text{on } \Gamma_p, \tag{2.4}$$

$$\boldsymbol{T} = -\mathrm{div}_p(\boldsymbol{M}) \quad \text{on } \Gamma_p, \tag{2.5}$$

$$\boldsymbol{M} = E_p I((1-\nu)\boldsymbol{e}_p(\boldsymbol{\nabla}_p u) + \nu \boldsymbol{\nabla}_p \cdot \boldsymbol{\nabla}_p u \boldsymbol{I}) \quad \text{on } \Gamma_p. \tag{2.6}$$

Here, all of the differential operators are acting in the plane Γ_p of the films. This is represented by the subscript p. For example, $\boldsymbol{\nabla}_p$ stands for the in-plane gradient operator and $\boldsymbol{e}_p(\boldsymbol{a}) = (\mathrm{grad}_p(\boldsymbol{a}) + (\mathrm{grad}_p(\boldsymbol{a}))^{\mathrm{T}})/2$ is the in-plane strain tensor with, in the present case, $\boldsymbol{a} = \boldsymbol{\nabla}_p u$. The transverse force and the bending moment tensor are respectively denoted as $\boldsymbol{T}$ and $\boldsymbol{M}$. The apparent Young's modulus of the films is given by $E_p = E/(1-\nu^2)$, where E is the Young's modulus and ν is the Poisson ratio. The inertia moment is given by $I = t^3/12$. It should be noted that the term $E_p I$ corresponds to the flexural stiffness, and the films (in vacuum) are loaded by their own inertia $\rho_p t\omega^2$, with $\rho_p t$ being the surface density of the films. We emphasise that under bending, the thickness of the films can be considered as constant so that they are deformed without undergoing volume variation.

As previously mentioned, we consider that the edges of the films, $\partial\Gamma_p$, are clamped to the solid boundary Γ_s, i.e.

$$u = 0 \quad \text{and} \quad \boldsymbol{\nabla}_p u \cdot \boldsymbol{n} = 0 \quad \text{on } \partial\Gamma_p, \tag{2.7}$$

where $\boldsymbol{n}$ is the outward-pointing normal vector of the edges $\partial\Gamma_p$.

Sound propagation in permeo-elastic materials is characterised by the interaction between the saturating fluid and the films. Consequently, the equations describing the out-of-plane displacement of the films and the fluid flow through the material are coupled. A two-way coupling is achieved as follows.

First, the boundary condition on the surface Γ_p expressing the continuity of fluid and film velocities on both faces of the films Γ_p^+ and Γ_p^- is added. The uniform out-of-plane displacement across the film thickness allows us to express the boundary condition as

$$\boldsymbol{v} = \mathrm{i}\omega u \boldsymbol{N} \quad \text{on } \Gamma_p, \tag{2.8}$$

where, by convention, $\boldsymbol{N}$ is the outward-pointing normal vector to Γ_p^+. It should be noted that the film kinematics imposes that the velocity of the fluid is orthogonal to the films.

Second, the transverse force equilibrium equation (2.4) is modified by the stress exerted by the fluid on the two faces of the films. The latter is given by $(\boldsymbol{\sigma}_f \cdot \boldsymbol{N}^+ - \boldsymbol{\sigma}_f \cdot \boldsymbol{N}^-)$. Hence, the normal component of the fluid loading on the films can be written as $[\boldsymbol{\sigma}_f \cdot \boldsymbol{N}] \cdot \boldsymbol{N}$, where $[\cdot]$ denotes the 'jump' across the interface Γ_p. Then, equation (2.4) becomes

$$\boldsymbol{\nabla}_p \cdot \boldsymbol{T} = -\rho_p t\omega^2 u - [\boldsymbol{\sigma}_f \cdot \boldsymbol{N}] \cdot \boldsymbol{N} \quad \text{on } \Gamma_p. \tag{2.9}$$

It must be noticed that due to the negligible thickness of the films, the momentum caused by the tangential stress exerted by the fluid does not modify the moment balance equation (2.5).

In summary, the local description is given by (2.1), (2.2), (2.9), (2.5), (2.6) and boundary conditions (2.3), (2.7) and (2.8). This is similar to that in Panasenko & Stavre (2012) for the case of viscous fluid–thin plate interaction and periodic flow, and that in Lebental & Bourquin (2012) for water–plate interaction in confined media. The next section deals with the physical analysis of the local description.

2.3. *Physical analysis*

This section presents the physical analysis of the local description. Assuming scale separation, we focus on describing the most general case for which all of the physical phenomena are present and interact at the local scale. The aim is to derive a general model that (i) captures the contribution of the local physics to the macroscopic behaviour of permeo-elastic media and (ii) reduces to degenerated models in which, for example, one of the mechanisms does not significantly contribute to the macroscopic acoustic behaviour.

As in long-wavelength sound propagation in conventional porous media (Auriault *et al.* 1985, 2009; Lafarge *et al.* 1997), the pressure fluctuates at the macroscopic scale, and, while the velocity and its rate of deviatoric deformation vary at the microscopic scale, the microscopic divergence itself is of the order of the macroscopic divergence, i.e.

$$\boldsymbol{\nabla} p = O\left(\frac{p}{L}\right), \quad \eta \boldsymbol{\nabla}^2 \boldsymbol{v} = O\left(\frac{\eta v}{l^2}\right) \quad \text{and} \quad \boldsymbol{\nabla} \cdot \boldsymbol{v} = O\left(\frac{v}{L}\right). \tag{2.10a–c}$$

The richest flow regime occurs when the viscous and inertial terms balance the pressure gradient. This means that the three terms in the oscillatory Stokes equation (2.1) are of the same order of magnitude (Auriault *et al.* 1985, 2009), i.e.

$$O\left(\frac{\eta v}{l^2}\right) = O(\rho_0 \omega v) = O\left(\frac{p}{L}\right). \tag{2.11}$$

In addition, the temporal relative variations of the pressure are balanced out by the rate of volume variations (Auriault *et al.* 1985, 2009), i.e.

$$O\left(\omega \frac{p}{\gamma P_0}\right) = O\left(\frac{v}{L}\right). \tag{2.12}$$

For permeo-elastic media, the case of interest occurs when the films are strongly interacting with the fluid. Due to the continuity of fluid and film velocities (2.8), one necessarily has that

$$O(v) = O(\omega u). \tag{2.13}$$

This implies that the velocity of the films varies at the local scale. In turn, this leads us to consider that the transverse force and the moment bending tensor also vary at the local scale, i.e.

$$O(M) = O\left(\frac{E_p I u}{l^2}\right), \quad O(T) = O\left(\frac{M}{l}\right), \quad \text{and} \quad O(\boldsymbol{\nabla}_p \cdot \boldsymbol{T}) = O\left(\frac{T}{l}\right). \tag{2.14a–c}$$

The most interesting case corresponds to elasto-inertial fluid–film interaction. According to the previous estimates, this leads us to consider that the terms in (2.9) are of the same order of magnitude, i.e.

$$O\left(\frac{T}{l}\right) = O(\rho_p t \omega^2 u) = O\left(\frac{\eta v}{l}\right) = O\left(\frac{l}{L} p\right). \tag{2.15}$$

The last two estimates are justified as follows. Since the deviatoric viscous stress varies at the microscopic scale, the jump of this quantity across the interface also fluctuates at the local scale, i.e. $O([\eta v/l]) = O(\eta v/l)$. However, since the pressure fluctuates at the macroscopic scale, the jump in pressure is assessed as $(p^+ - p^-)/l = O([p]/l) = O(p/L)$.

As a final remark, in accordance with (2.11), (2.15) and (2.13), the co-existence of inertial effects in both the fluid and the films leads to $O(\rho_p t\omega u\omega/l) = O(\rho_0\omega v)$, which results in $O(\rho_p t/h) = O(\rho_0)$.

2.4. *Homogenisation methodology*

The scale separation between the wavelength and the period size allows us to use the two-scale asymptotic homogenisation method (Sanchez-Palencia 1980; Auriault *et al.* 2009) to derive the equivalent macroscopic description. To represent the evolution at the two spatial scales, one can introduce the following two dimensionless space variables: $x/L = x^*$ and $x/l = y^*$, where x stands for the usual space variable. The space variables x^* and y^* are associated with the variations at the wavelength and period scales respectively. One can equivalently use the two dimensional space variables $x = Lx^*$ and $y = Ly^* = xL/l = \varepsilon^{-1}x$ by taking L as the reference length. It then follows that any quantity Q is considered to be a function of (x, y), i.e. $Q = Q(x, y)$. This brings as a consequence that the usual gradient operator $\boldsymbol{\nabla}_x$ is changed into $\boldsymbol{\nabla}_{(xy)} = \boldsymbol{\nabla}_x + \varepsilon^{-1}\boldsymbol{\nabla}_y$ (and $\boldsymbol{\nabla}^2_{(xy)} = \nabla^2_x + 2\varepsilon^{-1}\boldsymbol{\nabla}_{xy} + \varepsilon^{-2}\nabla^2_y$). To reflect the physics of the phenomena, the use of two space variables (x, y) should be combined with a rescaling of the usual equations based upon a single space variable. The reason for the rescaling lies in the fact that when expressed with the two space variables (x, y), the actual physical gradient of a quantity Q that varies at the large scale, i.e. $\boldsymbol{\nabla}_x Q$, becomes $\boldsymbol{\nabla}_{(xy)} Q$. On the other hand, if the quantity varies at the local scale, the actual physical gradient $\boldsymbol{\nabla}_y Q$ has to be expressed as $\varepsilon\boldsymbol{\nabla}_{(xy)} Q$. Therefore, the gradient of variables oscillating at the local scale should be rescaled. For instance, $\nabla^2\boldsymbol{v}$ should be rewritten as $\varepsilon^2\nabla^2_{(xy)}\boldsymbol{v}(x, y)$ to express that the fluid velocity actually varies at the pore scale.

Using the estimates identified in the physical analysis, equations (2.1), (2.2), (2.9), (2.5), (2.6) and boundary conditions (2.8), (2.3) and (2.7) are rewritten in the following two-space-variable formulation in rescaled form. It should be noted that we adopt the usual homogenisation convention which consists of keeping the same notation as for the single-space-variable formulation for both the variables and the gradient operator. Therefore, in (2.16)–(2.23), $\boldsymbol{\nabla}$ stands for $\boldsymbol{\nabla}_{(xy)}$, $\boldsymbol{v}$ represents $\boldsymbol{v}(x, y)$, etc.

$$\varepsilon^2\mathrm{div}(2\eta\boldsymbol{D}(\boldsymbol{v})) = \mathrm{i}\omega\rho_0\boldsymbol{v} + \boldsymbol{\nabla}p \quad \text{in } \Omega_f, \tag{2.16}$$

$$\mathrm{i}\omega\frac{p}{\gamma P_0} + \boldsymbol{\nabla}\cdot\boldsymbol{v} = 0 \quad \text{in } \Omega_f, \tag{2.17}$$

$$\boldsymbol{v} = \boldsymbol{0} \quad \text{on } \Gamma_s, \tag{2.18}$$

$$\boldsymbol{v} = \mathrm{i}\omega u\boldsymbol{N} \quad \text{on } \Gamma_p, \tag{2.19}$$

$$\varepsilon\boldsymbol{\nabla}_p\cdot\boldsymbol{T} = -\rho_p t\omega^2 u - \varepsilon[2\eta\boldsymbol{D}(\boldsymbol{v})\cdot\boldsymbol{N}]\cdot\boldsymbol{N} + \varepsilon^{-1}[p\boldsymbol{I}\cdot\boldsymbol{N}]\cdot\boldsymbol{N} \quad \text{on } \Gamma_p, \tag{2.20}$$

$$\boldsymbol{T} = -\varepsilon\mathrm{div}_p(\boldsymbol{M}) \quad \text{on } \Gamma_p, \tag{2.21}$$

$$\boldsymbol{M} = \varepsilon^2 E_p I((1-\nu)\boldsymbol{e}_p(\boldsymbol{\nabla}_p u) + \nu\boldsymbol{\nabla}_p\cdot\boldsymbol{\nabla}_p u\boldsymbol{I}) \quad \text{on } \Gamma_p, \tag{2.22}$$

$$u = 0 \quad \text{and} \quad \varepsilon\boldsymbol{\nabla}_p u\cdot\boldsymbol{n} = 0 \quad \text{on } \partial\Gamma_p. \tag{2.23}$$

It should be noted that in the rescaled system, the jump in pressure is explicitly of the order of the pressure $O(p)$. However, it has been shown in the previous section that, physically, the jump in pressure is one order smaller than the pressure. Therefore, to satisfy this physical estimation, the jump in pressure in (2.20) should be rescaled as $\varepsilon^{-1}[p] = O(p)$.

According to the standard homogenisation procedure, the physical variables are looked for in the form of asymptotic expansions in powers of the small parameter

ε as $Q(x, y) = \sum_{i=0}^{\infty} \varepsilon^i Q^{(i)}(x, y)$, where $Q = \boldsymbol{v}, p, u$. These are then substituted into (2.16)–(2.23) and the terms of the same order are identified. This procedure based upon the physical analysis ensures that the limiting description obtained when $\varepsilon \to 0$ keeps a physics of the same nature as in the real situation where the scale separation is finite.

2.5. *Fluid–structure interaction cell problem*

At ε^{-1}, it follows from the equations of conservation of momentum that $\nabla_y p^{(0)} = 0$ in Ω_f and $[p^{(0)}] = 0$ on Γ_p. This means that the pressure is a macroscopic variable, i.e. $p^{(0)} = p^{(0)}(x)$. According to the physical analysis, this result is consistent with the fact that the films are not loaded by the leading-order pressure.

Further identification leads to the following fluid–structure interaction cell problem (with $\boldsymbol{\sigma}_f^{(1)} = 2\eta \boldsymbol{D}_y(\boldsymbol{v}^{(0)}) - p^{(1)}\boldsymbol{I}$):

$$\mathrm{div}_y(\boldsymbol{\sigma}_f^{(1)}) = \mathrm{i}\omega\rho_0 \boldsymbol{v}^{(0)} + \nabla_x p^{(0)} \quad \text{in } \Omega_f, \tag{2.24}$$

$$\nabla_y \cdot \boldsymbol{v}^{(0)} = 0 \quad \text{in } \Omega_f, \tag{2.25}$$

$$\boldsymbol{v}^{(0)} = \boldsymbol{0} \quad \text{on } \Gamma_s, \tag{2.26}$$

$$\boldsymbol{v}^{(0)} = \mathrm{i}\omega u^{(0)} \boldsymbol{N} \quad \text{on } \Gamma_p, \tag{2.27}$$

$$\nabla_{yp} \cdot \boldsymbol{T}^{(0)} = -\rho_p t \omega^2 u^{(0)} - [\boldsymbol{\sigma}_f^{(1)} \cdot \boldsymbol{N}] \cdot \boldsymbol{N} \quad \text{on } \Gamma_p, \tag{2.28}$$

$$\boldsymbol{T}^{(0)} = -\mathrm{div}_{yp}(\boldsymbol{M}^{(0)}) \quad \text{on } \Gamma_p, \tag{2.29}$$

$$\boldsymbol{M}^{(0)} = E_p I((1-\nu)\boldsymbol{e}_{yp}(\nabla_{yp} u^{(0)}) + \nu \nabla_{yp} \cdot \nabla_{yp} u^{(0)} \boldsymbol{I}) = E_p I \mathcal{M}(u^{(0)}) \quad \text{on } \Gamma_p, \tag{2.30}$$

$$u^{(0)} = 0 \quad \text{and} \quad \nabla_{yp} u^{(0)} \cdot \boldsymbol{n} = 0 \quad \text{on } \partial\Gamma_p. \tag{2.31}$$

This linear problem, whose unknowns are $\boldsymbol{v}^{(0)}$, $p^{(1)}$ and $u^{(0)}$, is forced by the macroscopic pressure gradient $\nabla_x p^{(0)}$. To further investigate this cell problem, it is convenient to derive its associated variational formulation.

We consider the vectorial space $\mathcal{W}$ of complex velocity fields $\boldsymbol{w}$ defined in $\Omega_f \cup \Gamma_p$ such that $\boldsymbol{w}$ is Ω-periodic, divergence free $\nabla_y \cdot \boldsymbol{w} = 0$ in Ω_f, with $\boldsymbol{w} = 0$ on Γ_s, $\boldsymbol{w} = w\boldsymbol{N}$ on Γ_p, and $w = 0$ and $\nabla_{yp} w \cdot \boldsymbol{n} = 0$ on $\partial\Gamma_p$. To take advantage of the properties of a Hilbert space, let us introduce the following scalar product on $\mathcal{W}$ (it should be noted that $\overline{\boldsymbol{w}}$ is the complex conjugate of $\boldsymbol{w}$):

$$(\boldsymbol{v}, \boldsymbol{w}) = \int_{\Omega_f} \boldsymbol{D}_y(\boldsymbol{v}) : \boldsymbol{D}_y(\overline{\boldsymbol{w}})\, \mathrm{d}\Omega, \quad \|\boldsymbol{w}\|^2 = (\boldsymbol{w}, \overline{\boldsymbol{w}}). \tag{2.32}$$

This expression provides a norm since $\|\boldsymbol{w}\|^2 = 0$ implies that $\boldsymbol{D}_y(\boldsymbol{w}) = 0$. Therefore, $\boldsymbol{w}$ is a rigid-body field which reduces to $\boldsymbol{w} = 0$ when taking into account the boundary condition on Γ_s. Equipped with this norm, the space $\mathcal{W}$ is a Hilbert space.

The variational formulation of the fluid–structure interaction cell problem is obtained by (i) multiplying the equation of conservation of momentum in the fluid (2.24) by the conjugate of $\boldsymbol{w} \in \mathcal{W}$ and integrating it over Ω_f, (ii) multiplying the momentum balance of the film (2.28) (expressed in terms of the velocity of the films $v^{(0)} = \mathrm{i}\omega u^{(0)}$) by $\overline{w}$ and integrating it over Γ_p and (iii) adding the two integrals. Further use of the divergence theorem, boundary conditions on Γ_s and Γ_p, and periodicity leads to the following result (see appendix A, where the mathematical details of the derivation are provided):

$$\forall \boldsymbol{w} \in \mathcal{W}, \quad a(\boldsymbol{v}^{(0)}, \boldsymbol{w}) = b(\boldsymbol{w}), \tag{2.33}$$

where

$$a(\boldsymbol{v}^{(0)}, \boldsymbol{w}) = \overbrace{\eta \int_{\Omega_f} 2\boldsymbol{D}_y(\boldsymbol{v}^{(0)}) : \boldsymbol{D}_y(\overline{\boldsymbol{w}})\,\mathrm{d}\Omega}^{\mathcal{V}} + \overbrace{\mathrm{i}\omega\rho_0 \int_{\Omega_f} \boldsymbol{v}^{(0)} \cdot \overline{\boldsymbol{w}}\,\mathrm{d}\Omega}^{\mathcal{I}_f} + \underbrace{\mathrm{i}\omega\rho_p t \int_{\Gamma_p} v^{(0)}\overline{w}\,\mathrm{d}\Gamma}_{\mathcal{I}_p} + \underbrace{\frac{E_p I}{\mathrm{i}\omega} \int_{\Gamma_p} \mathcal{N}(v^{(0)}, w)\,\mathrm{d}\Gamma}_{\mathcal{E}}, \tag{2.34}$$

with

$$\mathcal{N}(v^{(0)}, w) = (1-\nu)\boldsymbol{e}_{yp}(\boldsymbol{\nabla}_{yp} v^{(0)}) : \boldsymbol{e}_{yp}(\boldsymbol{\nabla}_{yp}\overline{w}) + \nu \Delta_{yp} v^{(0)} \Delta_{yp}\overline{w} \tag{2.35}$$

and

$$b(\boldsymbol{w}) = -\int_{\Omega_f} \boldsymbol{\nabla}_x p^{(0)} \cdot \overline{\boldsymbol{w}}\,\mathrm{d}\Omega. \tag{2.36}$$

From now on, we will refer to $\mathcal{V}$, $\mathcal{I}_f$, $\mathcal{E}$ and $\mathcal{I}_p$ as the terms respectively associated with the effects of viscosity and inertia of the fluid, and elasticity and inertia of the films, as indicated in (2.34).

The form a in (2.33) is sesquilinear while b is semi-linear. In addition, by taking $\boldsymbol{w} = \boldsymbol{v}^{(0)}$ in (2.34), one obtains

$$a(\boldsymbol{v}^{(0)}, \boldsymbol{v}^{(0)}) = \eta \int_{\Omega_f} 2|\boldsymbol{D}_y(\boldsymbol{v}^{(0)})|^2\,\mathrm{d}\Omega + \mathrm{i}\omega\rho_0 \int_{\Omega_f} |\boldsymbol{v}^{(0)}|^2\,\mathrm{d}\Omega + \frac{E_p I}{\mathrm{i}\omega} \int_{\Gamma_p} ((1-\nu)|\boldsymbol{e}_{yp}(\boldsymbol{\nabla}_{yp} v^{(0)})|^2 + \nu|\Delta_{yp} v^{(0)}|^2)\,\mathrm{d}\Gamma + \mathrm{i}\omega\rho_p t \int_{\Gamma_p} |v^{(0)}|^2\,\mathrm{d}\Gamma. \tag{2.37}$$

The term a is a coercive form on $\mathcal{W}$ since $|a(\boldsymbol{v}^{(0)}, \boldsymbol{v}^{(0)})| \geqslant 2\eta\|\boldsymbol{v}^{(0)}\|$. The Lax–Milgram lemma ensures the existence and uniqueness of the solution $\boldsymbol{v}^{(0)}$ in Ω_f and, by continuity, that of $v^{(0)}$ on Γ_p.

Since (2.33) is a linear problem forced by the macroscopic pressure gradient, the solution $\boldsymbol{v}^{(0)}$ can be written as a linear combination of the three particular Ω-periodic fields $\boldsymbol{k}^J(y, \omega)$ corresponding to $\eta^{-1}\boldsymbol{\nabla}_x p^{(0)} = \boldsymbol{e}_J$, where the $\boldsymbol{e}_J$ (with $J = 1, 2, 3$) are the unitary basis vectors, i.e.

$$\boldsymbol{v}^{(0)} = -\frac{\widehat{\boldsymbol{k}}(y, \omega)}{\eta} \cdot \boldsymbol{\nabla}_x p^{(0)}, \quad \text{i.e.} \quad v_i^{(0)} = -\frac{\widehat{k}_i^J(y, \omega)}{\eta} \cdot (\boldsymbol{\nabla}_x p^{(0)})_J \quad \text{in } \Omega_f, \tag{2.38}$$

$$v^{(0)} = \boldsymbol{v}^{(0)} \cdot \boldsymbol{N} \quad \text{on } \Gamma_p, \tag{2.39}$$

where the tensor $\widehat{\boldsymbol{k}}(y, \omega)$ includes visco-elasto-inertial effects. It should be noted that (i) this quantity depends on the geometry of the material and the physical properties of the films and the saturating fluid, and (ii) the motion of the films is linearly related to the macroscopic pressure gradient.

From the fluid velocity field and the equation of conservation of momentum, one can deduce the expression of the pressure field as

$$p^{(1)} = -\widehat{\pi}^J(y, \omega) \cdot (\boldsymbol{\nabla}_x p^{(0)})_J + \widehat{p}^{(1)}(x) \quad \text{in } \Omega_f, \tag{2.40}$$

where the $\widehat{\pi}^J(y, \omega)$ are the particular solutions for $\eta^{-1}\boldsymbol{\nabla}_x p^{(0)} = \boldsymbol{e}_J$ and $\widehat{p}^{(1)}(x)$ is an integration constant.

Several remarks regarding the results presented in this section can be made as follows.

(i) The first and second integrals in the term $a(\boldsymbol{v}^{(0)}, \boldsymbol{v}^{(0)})$ in (2.37) respectively represent the viscous dissipative power and the inertial power developed in the fluid. The third and fourth integrals account for the elastic stored power and the inertial power in the films respectively. These powers are balanced by the one developed by the pressure gradient, which is accounted for by $b(\boldsymbol{v}^{(0)})$.

(ii) The terms associated with viscosity and inertial effects in $a(\boldsymbol{v}^{(0)}, \boldsymbol{v}^{(0)})$ (i.e. the first and second integrals) along with the term in $b(\boldsymbol{v}^{(0)})$ associated with the pressure gradient correspond to those appearing in the variational formulation of the cell problem found in conventional porous materials. Here, it is of interest to compare a permeo-elastic material with the two following conventional porous materials having the same rigid frame: (1) one in which extremely stiff films are attached and (2) another one where no films are attached. In these three materials, the kinematic conditions imposed on the velocity fields differ only by the condition set on Γ_p. The latter corresponds to the no-slip condition $\boldsymbol{v}^{(0)} = 0$ on Γ_p for extremely stiff films, $\boldsymbol{v}^{(0)} = v^{(0)}\boldsymbol{N}$ on Γ_p for elastic films, and continuous fluid velocity in the absence of films. Consequently, there is no direct correspondence between the classical and the present variational formulation as the spaces of solution differ. However, in the three cases, the velocity fields are continuous in $\Omega_f \cup \Gamma_p$. Regarding the fluid stress fields, these are continuous within the fluid space Ω_f but may differ on the two sides of Γ_p. However, since the films introduce internal solid boundaries, the condition of continuity across Γ_p does not have to be considered for the fluid phase. Due to these considerations about the smoothness of the fields in Ω_f, and taking into account the different kinematic restrictions, one obtains that the spaces of velocity fields, defined strictly in Ω_f, are structured as $W_r \subseteq \mathcal{W} \subseteq W$, where W_r and W are the spaces associated with the material with extremely stiff films and without films respectively. As a consequence, the static permeability (respectively high-frequency tortuosity) of the material with extremely stiff films is smaller (respectively larger) than that of the material with no films.

(iii) The presence of the films introduces two effects that are a direct consequence of the fluid–film interaction. These are represented by the elastic term $\mathcal{E}$, which does not appear in the conventional Darcy's cell problem and introduces an additional mechanism, and the inertial term $\mathcal{I}_p$, which is of a similar nature to that in the fluid.

(iv) In contrast to the usual visco-inertial description in conventional porous media which excludes the possibility of inner resonances, the fact that the elastic effects can be balanced out by the inertial ones can lead to inner resonances that result in atypical behaviour.

(v) Finally, we recall that in standard poroelasticity, the elastic effects are of different nature. Specifically, the solid displacement varies at the macroscopic scale so that the fluid flow cell problem is not affected by the deformation of the solid. This brings as a consequence that the visco-inertial permeability does not depend on the solid elasticity. On the other hand, the effective elasticity of the skeleton results from a cell problem defined in the solid domain and forced by the macroscopic strain and fluid pressure. Conversely, in permeo-elastic materials, the fluid flow is affected by the elastic deformation of the films, which is forced by the pressure gradient.

2.6. *Macroscopic acoustic description*

The leading-order mass balance equation is given by

$$\mathrm{i}\omega \frac{p^{(0)}}{\gamma P_0} + \boldsymbol{\nabla}_x \cdot \boldsymbol{v}^{(0)} + \boldsymbol{\nabla}_y \cdot \boldsymbol{v}^{(1)} = 0 \quad \text{in } \Omega_f. \tag{2.41}$$

Integration of this equation over Ω_f yields

$$\int_{\Omega_f} \mathrm{i}\omega \frac{p^{(0)}}{\gamma P_0}\,\mathrm{d}\Omega + \int_{\Omega_f} \nabla_x \cdot \boldsymbol{v}^{(0)}\,\mathrm{d}\Omega + \int_{\Omega_f} \nabla_y \cdot \boldsymbol{v}^{(1)}\,\mathrm{d}\Omega = 0. \tag{2.42}$$

The rightmost term in (2.42) can be written as a surface integral by using the divergence theorem. The resulting integral is null because of periodicity, null velocity $\boldsymbol{v}^{(1)} = 0$ on Γ_s and the continuity of the fluid velocity across the interface $\boldsymbol{v}^{(1)} \cdot \boldsymbol{N}^{+} = \boldsymbol{v}^{(1)} \cdot \boldsymbol{N}^{-} = v^{(1)}$ on Γ_p.

Thus, the macroscopic description is given by

$$\nabla_x \cdot \langle \boldsymbol{v}^{(0)} \rangle + \mathrm{i}\omega \frac{p^{(0)}}{\gamma P_0} = 0, \tag{2.43}$$

$$\langle \boldsymbol{v}^{(0)} \rangle = -\frac{\boldsymbol{k}(\omega)}{\eta} \cdot \nabla_x p^{(0)}, \tag{2.44}$$

where the average operator is defined by

$$\langle \cdot \rangle = \frac{1}{\Omega_f} \int_{\Omega_f} \cdot\,\mathrm{d}\Omega \tag{2.45}$$

and the effective visco-elasto-inertial permeability $\boldsymbol{k}(\omega)$ is calculated as

$$\boldsymbol{k}(\omega) = \langle \widehat{\boldsymbol{k}}(y, \omega) \rangle. \tag{2.46}$$

It should be noted that the permeability is related to the usual permeability $\underline{\boldsymbol{k}}$ determined by spatially averaging the velocity field with respect to the whole material volume through $\underline{\boldsymbol{k}} = \phi \boldsymbol{k}$. In this paper, we will systematically use the term permeability to refer to that calculated by spatially averaging the velocity field with respect to the pore volume, i.e. that calculated using the operator (2.45).

Equation (2.43) corresponds to the classical case of adiabatic mass balance in conventional rigid-frame porous material. This is because (i) the solid frame and the films in bending experience no volume variation and (ii) the thermal exchanges have been neglected for the sake of clarity in the presentation. It should be noted that accounting for heat exchanges would lead to replacement of the adiabatic bulk modulus γP_0 by the dynamic bulk modulus $K(\omega)$. The latter can be calculated, for example, using a semi-phenomenological model, as proposed in Lafarge *et al.* (1997).

Conversely, the fluid flow constitutive law given by (2.44) does not correspond to the classical dynamic Darcy's law since the elasto-inertial effects of the films are accounted for in the associated effective tensor $\boldsymbol{k}$, which is symmetric. This property is inherited from the symmetry of the form (2.34).

Depending on the frequency range and material parameters, it may be convenient to rewrite (2.44) in physically equivalent forms expressed in terms of the effective dynamic flow resistivity $\boldsymbol{H}(\omega)$ or apparent dynamic density $\boldsymbol{\rho}(\omega)$ tensors,

$$\boldsymbol{H}(\omega) \cdot \langle \boldsymbol{v}^{(0)} \rangle = -\nabla_x p^{(0)}, \tag{2.47}$$

$$-\omega^2 \boldsymbol{\rho}(\omega) \cdot \langle \boldsymbol{u}^{(0)} \rangle = -\nabla_x p^{(0)}, \tag{2.48}$$

where $\langle \boldsymbol{u}^{(0)} \rangle = \langle \boldsymbol{v}^{(0)} \rangle / \mathrm{i}\omega$ is the mean fluid displacement.

The effective dynamic flow resistivity and apparent dynamic density are related to the visco-elasto-inertial permeability by

$$\boldsymbol{\rho}(\omega) = \frac{\eta}{\mathrm{i}\omega}\boldsymbol{k}^{-1}(\omega) = \frac{\boldsymbol{H}(\omega)}{\mathrm{i}\omega}. \tag{2.49}$$

Combination of the macroscopic mass balance (2.43) and the constitutive fluid flow law (2.44) leads to the following wave equation:

$$\boldsymbol{\nabla}_x \cdot \left(\frac{\boldsymbol{k}(\omega)}{\eta} \cdot \boldsymbol{\nabla}_x p^{(0)} \right) = \mathrm{i}\omega \frac{p^{(0)}}{K(\omega)}. \tag{2.50}$$

Considering the case of isotropic permeo-elastic materials, one has that $\boldsymbol{k} = \mathcal{K}\boldsymbol{I}$. Then, the characteristic impedance Z_c, wavenumber k_c and speed of sound $\mathcal{C}$ through the material are given by

$$Z_c(\omega) = \sqrt{\frac{\eta}{\mathrm{i}\omega\mathcal{K}}K}, \quad k_c(\omega) = \omega\sqrt{\frac{\eta}{\mathrm{i}\omega\mathcal{K}}\frac{1}{K}} \quad \text{and} \quad \mathcal{C}(\omega) = \frac{\omega}{k_c(\omega)} = \sqrt{\frac{\mathrm{i}\omega\mathcal{K}}{\eta}K}. \tag{2.51a–c}$$

To understand the acoustical properties of permeo-elastic materials, it is required to investigate those of the visco-elasto-inertial permeability tensor. This is developed in the next section.

3. Properties of the visco-elasto-inertial permeability

This section deals with the analysis of the effective properties of permeo-elastic materials. In this type of material, the fluid flow is affected by three mechanisms of different nature, which are related to the effects of viscosity $\mathcal{V}$, elasticity $\mathcal{E}$ and inertia of the fluid and the films ($\mathcal{I}_f$ and $\mathcal{I}_p$). In general, these three mechanisms are involved and induce complex fluid flow regimes. To get an insight into this, the analysis of the behaviour will be carried out in two steps. In the first one, the different characteristic frequencies that determine the material behaviour will be identified. Second, asymptotic analyses with reference to the already identified characteristic frequencies will be conducted in an attempt to describe, in a simplified manner, the material behaviour in different regimes.

3.1. *Characteristic frequencies*

In contrast to the classical case of rigid-frame porous media, where only a visco-inertial characteristic frequency can be identified, in permeo-elastic materials, the three mechanisms involved give rise to at least three characteristic frequencies that determine the behaviour of the material. These frequencies can be estimated by considering each one of the three possible combinations of two mechanisms, i.e. visco-inertial, visco-elastic and elasto-inertial. Indeed, when only two of the mechanisms are involved, a specific fluid flow regime arises, which is characterised by a frequency that determines the transition between the two degenerated regimes driven by a single mechanism, i.e. purely viscous, elastic and inertial regimes.

3.1.1. *Visco-inertial characteristic frequency*

Let us consider first the case where the elastic effects $\mathcal{E}$ are negligible. In this visco-inertial regime, equation (2.33) evaluated at $\boldsymbol{w} = \boldsymbol{v}^{(0)}$ can be rewritten as

$$\langle 2\eta|\boldsymbol{D}_y(\boldsymbol{v}^{(0)})|^2\rangle + \mathrm{i}\omega\rho_0\langle|\boldsymbol{v}^{(0)}|^2\rangle + \mathrm{i}\omega\rho_p t\frac{1}{\Omega_f}\int_{\Gamma_p}|v^{(0)}|^2\,\mathrm{d}\Gamma = -\nabla_x p^{(0)}\cdot\langle\overline{\boldsymbol{v}}^{(0)}\rangle = \eta\langle\boldsymbol{v}^{(0)}\rangle\cdot\boldsymbol{k}^{-1}(\omega)\cdot\langle\overline{\boldsymbol{v}}^{(0)}\rangle. \quad (3.1)$$

From this equation, one can deduce that the real part of $\eta\boldsymbol{k}^{-1}(\omega)$ is the density of viscous dissipated power, while the imaginary part corresponds to the density of the kinetic power (for unitary flux).

In a close analogy to the Biot frequency in conventional porous materials, one can define a characteristic frequency ω_v that determines the transition from the viscous to the inertial regime. At this frequency, the viscous dissipated and kinetic powers are equal, i.e. the real and imaginary parts of $\boldsymbol{k}(\omega)$ have the same magnitude.

Focusing on the case of isotropic permeo-elastic media, the permeability at low frequency is denoted by $\mathcal{K}(\omega\to 0) = \mathcal{K}_0$ and the effective mass density at high frequency by $\rho(\omega\to\infty) = \varrho\alpha_\infty$, where α_∞ is a geometric factor of the fluid–film system representing its high-frequency tortuosity and $\varrho = \rho_0(1+\rho_p t\Gamma_p/\rho_0\Omega_f)$ is its mean density. Considering the low- and high-frequency limits of (3.1), these terms are given by

$$\frac{\eta}{\mathcal{K}_0} = \lim_{\omega\to 0}\frac{\langle 2\eta|\boldsymbol{D}_y(\boldsymbol{v}^{(0)})|^2\rangle}{|\langle\boldsymbol{v}^{(0)}\rangle|^2}, \quad (3.2)$$

$$\alpha_\infty = \lim_{\omega\to\infty}\left(\frac{\langle|\boldsymbol{v}^{(0)}|^2\rangle}{|\langle\boldsymbol{v}^{(0)}\rangle|^2} + \frac{\rho_p}{\rho_0}\frac{t}{\Omega_f}\frac{\displaystyle\int_{\Gamma_p}|v^{(0)}|^2\,\mathrm{d}\Gamma}{|\langle\boldsymbol{v}^{(0)}\rangle|^2}\right)\left(1+\frac{\rho_p t}{\rho_0}\frac{\Gamma_p}{\Omega_f}\right)^{-1}. \quad (3.3)$$

As in the conventional case, the visco-inertial characteristic frequency ω_v is estimated by considering that at this frequency, the viscous dissipation power is approximated by its low-frequency regime value, while the kinetic power by its high-frequency regime one. Equating these two terms leads to

$$\omega_v = \frac{\eta}{\mathcal{K}_0\varrho\alpha_\infty}. \quad (3.4)$$

3.1.2. *Visco-elastic characteristic frequency*

Let us now consider the case where the inertial effects $\mathcal{I}_f$ and $\mathcal{I}_p$ are negligible. In this visco-elastic regime, equation (2.33) evaluated at $\boldsymbol{w} = \boldsymbol{v}^{(0)}$ can be rewritten as

$$\langle 2\eta|\boldsymbol{D}_y(\boldsymbol{v}^{(0)})|^2\rangle + \frac{E_p I}{\mathrm{i}\omega}\frac{1}{\Omega_f}\int_{\Gamma_p}\mathcal{N}(v^{(0)},v^{(0)}) = -\nabla_x p^{(0)}\cdot\langle\overline{\boldsymbol{v}}^{(0)}\rangle = \eta\langle\boldsymbol{v}^{(0)}\rangle\cdot\boldsymbol{k}^{-1}(\omega)\cdot\langle\overline{\boldsymbol{v}}^{(0)}\rangle. \quad (3.5)$$

This equation shows that in the visco-elastic regime, the real part of $\eta\boldsymbol{k}^{-1}(\omega)$ is the density of viscous dissipated power, while the imaginary part corresponds to the density of the elastic power in the films (for unitary flux).

One can define a characteristic frequency ω_e that determines whether the viscous or elastic effects dominate. At this frequency, the viscous dissipated power and elastic power match, which occurs in this regime when the real and imaginary parts of $\boldsymbol{k}(\omega)$ have the same magnitude.

For simplicity, we consider again isotropic permeo-elastic media. When the viscous dissipated power (i.e. the first term on the left-hand side of (3.5)) vanishes, one obtains that the effective permeability tends to

$$\lim_{\eta\to 0}\frac{\mathcal{K}}{\eta}=\frac{\mathrm{i}\omega}{E_pI\theta},\quad \text{with } \theta=\Theta|_{\eta\to 0}\quad\text{and}\quad \Theta=\frac{\dfrac{1}{\Omega_f}\displaystyle\int_{\Gamma_p}\mathcal{N}(v^{(0)},v^{(0)})}{|\langle \boldsymbol{v}^{(0)}\rangle|^2},\tag{3.6a,b}$$

where the parameter θ is a geometrical factor related to the deformation of the films which can be estimated, applying a dimensional analysis to (2.35) and (3.6), as of the order of $\theta=O(\Gamma_p/\Omega_f h^4)$.

It should be noted that the permeo-elastic constitutive law (3.6) takes the form of an elastic constitutive law determined by the film properties, i.e.

$$\langle \boldsymbol{u}^{(0)}\rangle E_pI\theta=-\boldsymbol{\nabla}_x p^{(0)}.\tag{3.7}$$

Following the same approach as in the previous case, one deduces that the visco-elastic characteristic frequency is estimated by

$$\omega_e=\frac{\mathcal{K}_0}{\eta}E_pI\theta=O\left(\frac{E_p}{\eta}\left(\frac{t}{h}\right)^3\right).\tag{3.8}$$

It should be noted that this estimation has made use of the estimations of θ, $\mathcal{K}_0=O(l^2)$ and $I=O(t^3)$.

3.1.3. *Elasto-inertial characteristic frequencies*

We now consider the case where the viscous effects $\mathcal{V}$ can be disregarded. From (3.9), which is obtained by evaluating (2.33) at $\boldsymbol{w}=\boldsymbol{v}^{(0)}$, two elasto-inertial regimes will be identified

$$\frac{E_pI}{\mathrm{i}\omega}\frac{1}{\Omega_f}\int_{\Gamma_p}\mathcal{N}(v^{(0)},v^{(0)})\,\mathrm{d}\Gamma+\mathrm{i}\omega\rho_0\left(\langle|\boldsymbol{v}^{(0)}|^2\rangle+\frac{\rho_p}{\rho_0}\frac{t}{\Omega_f}\int_{\Gamma_p}|v^{(0)}|^2\,\mathrm{d}\Gamma\right)=-\boldsymbol{\nabla}_x p^{(0)}\cdot\langle\overline{\boldsymbol{v}}^{(0)}\rangle.\tag{3.9}$$

This formulation shows that the elastic and inertial effects (in both the fluid and the films) can balance each other at certain frequencies. These correspond to the resonances of the coupled fluid–film system. Attention is paid to the fundamental frequency ω_g, which can be estimated using a dimensional analysis as

$$\omega_g^2=\frac{E_pI\theta_g}{\varrho\alpha_\infty}=\omega_e\omega_v\frac{\theta_g}{\theta},\tag{3.10}$$

where $\theta_g=\Theta|_{\omega\to\omega_g}$ is a geometrical factor that accounts for the modal shape of the films. It should be noted that (3.10) and (3.6) constitute an implicit system. Hence, it is generally not possible to give an explicit expression but an estimation of the order of magnitude of $\theta_g=O(\Gamma_p/h^4\Omega_f)=O(\theta)$.

In order to reveal the behaviour of the material at ω_g, one can use (2.44), (3.6) and (3.3) to rewrite the variational form (2.33), for isotropic materials, as

$$\langle \boldsymbol{v}^{(0)} \rangle \cdot \langle \overline{\boldsymbol{v}}^{(0)} \rangle \frac{E_p I \theta}{\mathrm{i}\omega\eta} \frac{\theta_g}{\theta} + \langle \boldsymbol{v}^{(0)} \rangle \cdot \langle \overline{\boldsymbol{v}}^{(0)} \rangle \frac{\mathrm{i}\omega\varrho\alpha_\infty}{\eta} = -\frac{\boldsymbol{\nabla}_x p^{(0)}}{\eta} \cdot \langle \overline{\boldsymbol{v}}^{(0)} \rangle = \langle \boldsymbol{v}^{(0)} \rangle \cdot \mathcal{K}^{-1}(\omega) \cdot \langle \overline{\boldsymbol{v}}^{(0)} \rangle, \tag{3.11}$$

where the parameters α_∞ and θ_g take specific values around the frequency of interest. Then, by simplifying the velocity terms, one can estimate the dynamic elasto-inertial permeability as

$$\mathcal{K}(\omega) \cong \mathcal{K}_0 \frac{\omega_v}{\mathrm{i}\omega} \frac{1}{1 - \dfrac{\omega_e \omega_v}{\omega^2} \dfrac{\theta_g}{\theta}}, \tag{3.12}$$

which, considering the dependence of ω_g on ω_e and ω_v, leads to the following constitutive law:

$$\langle \boldsymbol{v}^{(0)} \rangle \cong -\frac{\mathcal{K}_0}{\eta} \frac{\omega_v}{\mathrm{i}\omega} \frac{1}{1 - \dfrac{\omega_g^2}{\omega^2}} \cdot \boldsymbol{\nabla}_x p^{(0)}. \tag{3.13}$$

This equation allows us to conclude that at the resonance frequency ω_g, the elasto-inertial permeability tends to infinity. Consequently, the apparent dynamic density tends to zero. Physically, this means that the averaged velocity takes very large values in response to a finite pressure gradient.

It must be emphasised that the parameters α_∞ and θ_g in (3.11) take specific values around the resonance frequency ω_g. At lower frequencies, the behaviour of the fluid–film system is mainly determined by the inertia of the fluid, which is characterised by a tortuosity factor α'_∞, i.e. the elasto-inertial permeability behaves as $\mathcal{K}(\omega) \cong \mathcal{K}_0 \omega'_v / \mathrm{i}\omega$, where $\omega'_v = \eta / \rho_0 \mathcal{K}_0 \alpha'_\infty$. This expression shows that the imaginary part of the elasto-inertial permeability is negative and its magnitude is a decreasing function of frequency. As the frequency increases, this response overlaps with that described by (3.13). Such an overlap, which is a product of the atypical modification of the effective inertia of the fluid–film system by the elasticity and inertia of the films, leads to the identification of a characteristic frequency ω_0 at which the elasto-inertial permeability becomes null, while the apparent dynamic density becomes singular. The frequency ω_0 can be estimated from (3.14) and is given by (3.15).

$$\mathcal{K}(\omega_0) \cong \mathcal{K}_0 \frac{\omega_v}{\mathrm{i}\omega_0} \left(\frac{\omega'_v}{\omega_v} + \frac{1}{1 - \dfrac{\omega_g^2}{\omega_0^2}} \right) = 0, \tag{3.14}$$

$$\omega_0 = \frac{\omega_g}{\sqrt{1 + \dfrac{\omega_v}{\omega'_v}}} = \frac{\omega_g}{\sqrt{1 + \dfrac{\rho_0}{\varrho} \dfrac{\alpha'_\infty}{\alpha_\infty}}}. \tag{3.15}$$

It should be noted that these atypical situations are exclusive to the elasto-inertial regime. In visco-inertial or visco-elastic regimes, the phase shift between the two respective mechanisms prevents the occurrence of resonance. This brings as a consequence that the effective permeability does not present poles.

Using the expressions of the characteristic frequencies, the variational formulation (2.33) can be rewritten in the following equivalent form:

$$\forall \boldsymbol{w} \in \mathcal{W}, \quad A(\boldsymbol{v}^{(0)}, \boldsymbol{w}) = B(\boldsymbol{w}), \tag{3.16}$$

where

$$\begin{aligned} A(\boldsymbol{v}^{(0)}, \boldsymbol{w}) \;=\; & \mathcal{K}_0 \int_{\Omega_f} 2\boldsymbol{D}_y(\boldsymbol{v}^{(0)}) : \boldsymbol{D}_y(\overline{\boldsymbol{w}})\, \mathrm{d}\Omega + \frac{\mathrm{i}\omega}{\omega_v} \frac{1}{\alpha_\infty \varrho} \int_{\Omega_f \cup \Gamma_p} \widetilde{\rho} \boldsymbol{v}^{(0)} \cdot \overline{\boldsymbol{w}}\, \mathrm{d}\Omega \\ & + \frac{\omega_e}{\mathrm{i}\omega} \frac{1}{\theta} \int_{\Gamma_p} \mathcal{N}(v^{(0)}, w)\, \mathrm{d}\Gamma \end{aligned} \tag{3.17}$$

and

$$B(\boldsymbol{w}) = -\frac{\mathcal{K}_0}{\eta} \nabla_x p^{(0)} \cdot \int_{\Omega_f} \overline{\boldsymbol{w}}\, \mathrm{d}\Omega. \tag{3.18}$$

Here, we have introduced the local density distribution $\widetilde{\rho} = \rho_0 + \rho_p t \delta_{\Gamma_p}$, where δ_{Γ_p} is the Dirac distribution associated with the film surface Γ_p. It should be noted that the mean density of the fluid–film system is given by $\varrho = \Omega_f^{-1} \int_{\Omega_f \cup \Gamma_p} \widetilde{\rho}\, \mathrm{d}\Omega$.

Alternatively, introducing the elasto-inertial frequency ω_g, A can be expressed as

$$\begin{aligned} A(\boldsymbol{v}^{(0)}, \boldsymbol{w}) \;=\; & \frac{\omega_e}{\mathrm{i}\omega} \frac{\theta_g}{\theta} \left(\frac{1}{\theta_g} \int_{\Gamma_p} \mathcal{N}(v^{(0)}, w)\, \mathrm{d}\Gamma - \frac{\omega^2}{\omega_g^2} \int_{\Omega_f \cup \Gamma_p} \frac{\widetilde{\rho}}{\rho_0} \boldsymbol{v}^{(0)} \cdot \overline{\boldsymbol{w}}\, \mathrm{d}\Omega \right) \\ & + \mathcal{K}_0 \int_{\Omega_f} 2\boldsymbol{D}_y(\boldsymbol{v}^{(0)}) : \boldsymbol{D}_y(\overline{\boldsymbol{w}})\, \mathrm{d}\Omega. \end{aligned} \tag{3.19}$$

Considering the complexity of the possible regimes in permeo-elastic media, it is convenient to investigate them through asymptotic analyses. These will be performed by expanding the local solutions in terms of dimensionless parameters identified in (3.17) and (3.19). In the next sections, we will consider the case of quasi-rigid films (i.e. $\omega/\omega_e \to 0$) and extremely flexible films (i.e. $\omega_e/\omega \to 0$) in both viscous (i.e. $\omega/\omega_v \to 0$) and inertial regimes (i.e. $\omega_v/\omega \to 0$).

We have the following remarks.

(i) We emphasise that a mixed regime in which viscous, inertial and elastic effects are of a similar order of magnitude exists. In this case, highly damped resonances can be observed, as will be shown numerically further below. It should be noted, however, that no analytical estimation of the characteristic frequency associated with this phenomenon can be provided. This is because the effective properties of the material cannot be approximated by their asymptotic values in this mixed regime.

(ii) For anisotropic materials, $\mathcal{K}_0$, α_∞, θ and θ_g are no longer scalars and have to be replaced by tensors. In such a case, the estimates of the characteristic frequencies take the same functional form but their parameters are assessed by the norm of the respective tensors involved. For simplicity, we have kept the scalar notation throughout § 3.1 to express the norm of the tensors, which is an approximation valid as long as the material is moderately anisotropic.

3.2. *Quasi-rigid films*

The behaviour of the effective properties of permeo-elastic materials is investigated using an asymptotic analysis. First, a dimensionless parameter $\alpha = \mathrm{i}\omega/\omega_e$ is identified from the variational formulation (3.16). The parameter α tends to zero when $\omega \ll \omega_e$. This is satisfied when either $E_p I \to \infty$, which corresponds to the case of quasi-rigid films, or $\omega \to 0$. This situation leads to a specific fluid–film interaction cell problem, as detailed in appendix B. The analysis is performed by expressing the local fields in the form of expansion series of the type $\boldsymbol{v}^{(0)} = \sum_{i=0}^{\infty} \alpha^i \boldsymbol{v}^{[i]}$, etc. The solution of the resulting problems at the first two orders of expansion in α yields for $\omega/\omega_e \ll 1$ (see appendix B for the details of the resolution)

$$\langle \boldsymbol{v}^{(0)} \rangle \cong -\left(\frac{\boldsymbol{k}_r(\omega)}{\eta} + \frac{\mathrm{i}\omega}{\omega_e} \frac{\boldsymbol{B}_r(\omega)}{\eta} \right) \cdot \boldsymbol{\nabla}_x p^{(0)} = -\left(\frac{\boldsymbol{k}_r(\omega)}{\eta} + \frac{\mathrm{i}\omega}{E_p} \frac{\boldsymbol{B}_r(\omega)}{I\mathcal{K}_0\theta} \right) \cdot \boldsymbol{\nabla}_x p^{(0)}, \quad (3.20)$$

where $\boldsymbol{k}_r(\omega)$ represents the standard dynamic permeability of a material with perfectly rigid films. The symmetric tensor $\boldsymbol{B}_r(\omega)$ (in m^2) is related to the fluid flow generated by the elastic motion of the films in response to the excitation by the fluid flow at the leading order (at α^0).

From (3.20), it is concluded that (i) the elasticity of the films acts as a corrector of the permeability and (ii) the classical dynamic Darcy's law is recovered for large values of the Young's modulus and at low frequencies.

Equation (3.20) can be written in the alternative forms (2.47) and (2.48). These will be used in §§ 3.2.1–3.2.3 to investigate the response of the fluid–film system in different fluid flow regimes.

$$-\boldsymbol{\nabla}_x p^{(0)} = \boldsymbol{H}_r(\omega) \cdot \langle \boldsymbol{v}^{(0)} \rangle \cong \eta \boldsymbol{k}_r^{-1}(\omega) \left(\boldsymbol{I} - \frac{\mathrm{i}\omega}{\omega_e} \boldsymbol{B}_r(\omega) \boldsymbol{k}_r^{-1}(\omega) \right) \cdot \langle \boldsymbol{v}^{(0)} \rangle, \quad (3.21)$$

$$-\boldsymbol{\nabla}_x p^{(0)} = -\omega^2 \boldsymbol{\rho}_r(\omega) \cdot \langle \boldsymbol{u}^{(0)} \rangle \cong -\omega^2 \eta \boldsymbol{k}_r^{-1}(\omega) \left(\frac{\boldsymbol{I}}{\mathrm{i}\omega} - \frac{1}{\omega_e} \boldsymbol{B}_r(\omega) \boldsymbol{k}_r^{-1}(\omega) \right) \cdot \langle \boldsymbol{u}^{(0)} \rangle. \quad (3.22)$$

In what follows, the analysis is conducted for an isotropic material (or for a preferential flow direction), i.e. the tensors involved become scalar. For example, the viscous permeability tensor reads as $\boldsymbol{k}_r(\omega) = \mathcal{K}_r(\omega)\boldsymbol{I}$. The analysis will be made with reference to figure 2. This figure shows a conceptual diagram representing the asymptotic behaviour of permeo-elastic materials with respect to the visco-inertial frequency ω_{vr} for the case $\omega \ll \omega_e$. It will become apparent throughout the next subsections under what conditions these regimes are achieved.

3.2.1. *Quasi-rigid films – visco-elastic regime ($a_1 : \mathcal{V} + \mathcal{E}$)*

For frequencies much smaller than the viscous characteristic frequency, i.e. $\omega \ll \omega_{vr} = \eta/\mathcal{K}_{r0}\rho_0\alpha_{\infty r}$, equation (3.20) becomes (with $G_i = -\boldsymbol{\nabla}_x p^{(0)} \cdot \boldsymbol{e}_i$ and $\omega \ll \omega_e$)

$$\langle \boldsymbol{v}_i^{(0)} \rangle \cong \frac{\mathcal{K}_{r0}}{\eta} \left(1 + \frac{\mathrm{i}\omega}{\omega_e} \frac{B_{r0}}{\mathcal{K}_{r0}} \right) G_i. \quad (3.23)$$

This equation can be rewritten in the alternative form (2.47) as

$$\frac{\mu_{a_1}(\omega)}{\mathcal{K}_{r0}} \langle \boldsymbol{v}_i^{(0)} \rangle \cong G_i, \quad \text{with} \quad \frac{1}{\mu_{a_1}(\omega)} = \frac{1}{\eta} + \frac{\mathrm{i}\omega}{\omega_e \eta} \frac{B_{r0}}{\mathcal{K}_{r0}}. \quad (3.24)$$

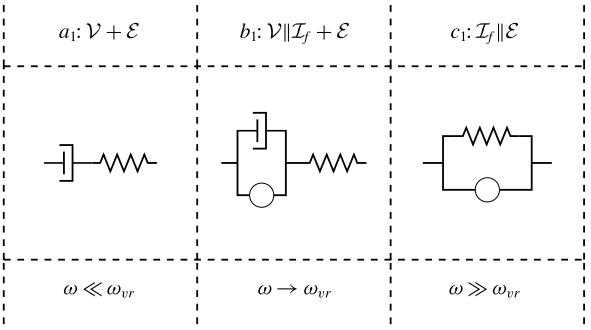

FIGURE 2. Rheological diagram representing the combination of dashpot ($\mathcal{V}$, ⊣⊢), spring ($\mathcal{E}$, -WW-) and mass ($\mathcal{I}_f$, ○) describing the acoustic behaviour of permeo-elastic materials with respect to the visco-inertial frequency ω_{vr} for the case $\omega \ll \omega_e$ (i.e. quasi-rigid films).

This equation shows that the flow is characterised by (i) the standard intrinsic permeability of the pore space with the films being perfectly rigid, $\mathcal{K}_{r0}$, and (ii) a saturating effective fluid that behaves rheologically as a Maxwell visco-elastic fluid (Boutin & Auriault 1990; López de Haro, Del Río & Whitaker 1996) with parameter $\mu_{a1}(\omega)$. This parameter corresponds to a dashpot of viscosity η connected in series with a stiff spring $E_{a_1} = \omega_e \eta \mathcal{K}_{r0}/B_{r0} = O(E_p I/h^3)$. This behaviour is represented by a_1 (i.e. $\mathcal{V}+\mathcal{E}$) in figure 2. The combination in series of the elements is consistent with the fact that the small deformation of the stiff films results from the stress imposed by the fluid flow. Furthermore, the fluid–film system behaviour can be alternatively analysed by rewriting (3.24) as

$$\left(\frac{1}{R_{a_1}} + \frac{1}{\dfrac{k_{a_1}}{\mathrm{i}\omega}}\right)^{-1} \langle \boldsymbol{v}_i^{(0)} \rangle = \left(\frac{1}{\dfrac{\eta}{\mathcal{K}_{r0}}} + \frac{1}{\dfrac{\omega_e \eta}{\mathrm{i}\omega B_{r0}}}\right)^{-1} \langle \boldsymbol{v}_i^{(0)} \rangle \cong G_i, \tag{3.25}$$

where the resistivity is given by $R_{a_1} = \eta/\mathcal{K}_{r0} = H_{r0}$ and the elasticity is represented by the stiff spring $k_{a_1} = \omega_e \eta / B_{r0} = E_p I \theta \mathcal{K}_0 / B_{r0}$.

The effective dynamic flow resistivity of the material for $\omega \ll \omega_{vr}$ and $\omega \ll \omega_e$ is then given by

$$H_{a_1}(\omega) \cong H_{r0}\left(1 - \frac{\mathrm{i}\omega}{\omega_e}\frac{B_{r0}}{\mathcal{K}_{r0}}\right). \tag{3.26}$$

This expression shows that the imaginary part of the effective dynamic flow resistivity takes negative values due to the contribution of the elasticity of the films. When using the positive convention $\mathrm{e}^{\mathrm{i}\omega t}$, as in this work, such a behaviour does not exist in conventional porous materials. The negativity of the imaginary part of the effective dynamic flow resistivity leads to a negative real part of the apparent dynamic density, as shown in (3.27). It is worth mentioning both that this behaviour has been observed in the so-called acoustic metamaterials (see, for example, the review papers by Cummer, Christensen & Alù 2016 and Ma & Sheng 2016) and that the homogenisation-based approach used in this work can provide a way of assessing their acoustical properties.

$$\rho_{a_1}(\omega) \cong -\frac{H_{r0}}{\omega_e}\frac{B_{r0}}{\mathcal{K}_{r0}} + \frac{H_{r0}}{\mathrm{i}\omega}. \tag{3.27}$$

3.2.2. *Quasi-rigid films – visco-elasto-inertial regime* ($b_1 : \mathcal{V} \parallel \mathcal{I}_f + \mathcal{E}$)

When the fluid flow enters into the visco-inertial regime, the effects of the inertia of the fluid start to be manifested. In this regime, equation (3.20) takes the following form valid for $\omega \ll \omega_e$ and $\omega < \omega_{vr}$:

$$\langle \boldsymbol{v}_i^{(0)} \rangle \cong \frac{\mathcal{K}_{r0}}{\eta} \left(1 + \mathrm{i}\omega \left(\frac{1}{\omega_e} \frac{B_{r0}}{\mathcal{K}_{r0}} - \frac{1}{\omega_{vr}} \frac{\alpha_{r0}}{\alpha_{\infty r}} \right) \right) G_i, \tag{3.28}$$

where α_{r0} is the static tortuosity (Pride, Morgan & Gangi 1993).

This equation can be rewritten as

$$\frac{\mu_{b_1}(\omega)}{\mathcal{K}_{r0}} \langle \boldsymbol{v}_i^{(0)} \rangle \cong G_i, \quad \text{with} \quad \frac{1}{\mu_{b_1}(\omega)} = \frac{1}{\eta + \mathrm{i}\omega \dfrac{\eta \alpha_{r0}}{\omega_{vr} \alpha_{\infty r}}} + \frac{\mathrm{i}\omega B_{r0}}{\omega_e \eta \mathcal{K}_{r0}}. \tag{3.29}$$

The fluid flow is characterised by (i) the standard intrinsic permeability of the pore space with the films being perfectly rigid, $\mathcal{K}_{r0}$, and (ii) a saturating effective fluid that behaves as a visco-elasto-inertial fluid with effective modulus $\mu_{b_1}(\omega)$.

The following alternative form allows us to conclude that the fluid–film system behaves as a parallel dashpot–mass system (with $R_{b_1} = R_{a_1}$ and $m_{b_1} = \eta \alpha_{r0} / \mathcal{K}_{r0} \omega_{vr} \alpha_{\infty r} = \rho_0 \alpha_{r0}$) connected in series to a stiff spring ($k_{b_1} = k_{a_1}$). This behaviour is represented by b_1 (i.e. $\mathcal{V} \parallel \mathcal{I}_f + \mathcal{E}$) in figure 2.

$$\left(\frac{1}{R_{b_1} + \mathrm{i}\omega m_{b_1}} + \frac{1}{\dfrac{k_{b_1}}{\mathrm{i}\omega}} \right)^{-1} \langle \boldsymbol{v}_i^{(0)} \rangle = \left(\frac{1}{\dfrac{\eta}{\mathcal{K}_{r0}} + \mathrm{i}\omega \dfrac{\alpha_{r0} \eta}{\omega_{vr} \alpha_{\infty r} \mathcal{K}_{r0}}} + \frac{1}{\dfrac{\omega_e \eta}{\mathrm{i}\omega B_{r0}}} \right)^{-1} \langle \boldsymbol{v}_i^{(0)} \rangle \cong G_i. \tag{3.30}$$

The effective dynamic flow resistivity and apparent dynamic density are given by

$$H_{b_1}(\omega) \cong H_{r0} + \frac{\mathrm{i}\omega}{\omega_{vr}} H_{r0} \frac{\alpha_{r0}}{\alpha_{\infty r}} \left(1 - \frac{\omega_{vr}}{\omega_e} \frac{B_{r0}}{\mathcal{K}_{r0}} \frac{\alpha_{\infty r}}{\alpha_{r0}} \right), \tag{3.31}$$

$$\rho_{b_1}(\omega) \cong \frac{H_{r0}}{\omega_{vr}} \frac{\alpha_{r0}}{\alpha_{\infty r}} \left(1 - \frac{\omega_{vr}}{\omega_e} \frac{B_{r0}}{\mathcal{K}_{r0}} \frac{\alpha_{\infty r}}{\alpha_{r0}} \right) + \frac{H_{r0}}{\mathrm{i}\omega}. \tag{3.32}$$

Considering the real part of (3.32), one can conclude that the fluid–film system behaves as an effective Maxwell fluid when the elastic effects dominate over those of the inertia of the fluid at low frequencies. Such a situation is observed when $\omega_{vr}/\omega_e > \mathcal{K}_{r0} \alpha_{r0} / B_{r0} \alpha_{\infty r} = O(1)$. The opposite case, i.e. elasticity effects weaker than inertial ones, leads to the fluid–film system behaving as an effective Newtonian fluid with a modified static tortuosity that accounts for the weak elastic effects. On the other hand, the real part of the apparent dynamic density can become null if $\omega_e B_{r0} \alpha_{\infty r} / \omega_{vr} \mathcal{K}_{r0} \alpha_{r0} = O(1)$. This condition determines the transition from elasticity- to inertia-dominated behaviour or from negative to positive real part of the apparent dynamic density.

3.2.3. *Quasi-rigid films – elasto-inertial regime* ($c_1 : \mathcal{I}_f \parallel \mathcal{E}$)

Viscosity effects can be disregarded for frequencies $\omega \gg \omega_{vr}$. Then, keeping in mind that $\omega \ll \omega_e$, equation (3.20) can be approximated by

$$\langle \boldsymbol{v}_i^{(0)} \rangle \cong \frac{\mathcal{K}_{r0}}{\eta} \left(\frac{\omega_{vr}}{\mathrm{i}\omega} + \frac{\mathrm{i}\omega}{\omega_e} \frac{B_{r\infty}}{\mathcal{K}_{r0}} \right) G_i. \tag{3.33}$$

Substituting the value of $B_{r\infty}$ given by (B 25), one obtains

$$\left(\mathrm{i}\omega m_{c_1} + \frac{k_{c_1}}{\mathrm{i}\omega}\right)\langle \boldsymbol{v}_i^{(0)}\rangle = \left(\mathrm{i}\omega\rho_0\alpha_{r\infty} + \frac{E_pI\theta}{\mathrm{i}\omega}\right)\langle \boldsymbol{v}_i^{(0)}\rangle \cong G_i. \tag{3.34}$$

This equation indicates that the fluid–film system behaves as a mass $m_{c_1} = \rho_0\alpha_{\infty r}$ and a spring $k_{c_1} = E_pI\theta$ connected in parallel. This case corresponds to c_1 (i.e. $\mathcal{I}_f \parallel \mathcal{E}$) in figure 2.

The effective dynamic flow resistivity and apparent dynamic density are respectively given by

$$H_{c_1}(\omega) \cong \mathrm{i}\omega\frac{H_{r0}}{\omega_{vr}}\left(1 - \frac{\omega_e\omega_{vr}}{\omega^2}\frac{\mathcal{K}_{r0}}{\mathcal{K}_0}\right), \tag{3.35}$$

$$\rho_{c_1}(\omega) \cong \frac{H_{r0}}{\omega_{vr}}\left(1 - \frac{\omega_e\omega_{vr}}{\omega^2}\frac{\mathcal{K}_{r0}}{\mathcal{K}_0}\right). \tag{3.36}$$

This equation shows that the apparent dynamic density becomes significantly influenced by the elasticity of the films, while in conventional porous materials it is only determined by the inertia of the fluid. The modification appears as a corrector that is inversely proportional to the square of frequency. It is worth noting that when the viscosity effects (i.e. $\omega \gg \omega_{vr}$) are negligible, the real part of the apparent dynamic density will tend to zero as $\omega \to \sqrt{k_{c_1}/m_{c_1}}$, provided that $\omega \ll \omega_e$.

3.3. *Very flexible films*

The same approach as in § 3.2 is followed in this section to investigate the behaviour of very flexible films. This situation can be studied by considering a small parameter $\beta = \omega_e/\mathrm{i}\omega \to 0$ identified from (3.16). This condition is satisfied when either $E_pI \to 0$ or $\omega \to \infty$. As in the previous section, the variables are looked for as expansion series but now in terms of β. The solution of the resulting problems at the first two orders of expansion in β yields for $\omega \gg \omega_e$ (see appendix C for the details of the resolution)

$$\langle \boldsymbol{v}^{(0)}\rangle \cong -\left(\frac{\boldsymbol{k}_s(\omega)}{\eta} - \frac{\omega_e}{\mathrm{i}\omega}\frac{\boldsymbol{B}_s(\omega)}{\eta}\right)\cdot\boldsymbol{\nabla}_x p^{(0)}, \tag{3.37}$$

where $\boldsymbol{k}_s(\omega)$ is the dynamic permeability of a material slightly different from one without films since a condition of normal flow on the films is imposed and its high-frequency behaviour is determined by the inertia of the fluid and that of the films. The term $\boldsymbol{B}_s(\omega)$ represents the additional flow required to equilibrate the films which are undergoing deformation imposed by the fluid flow at the leading order (i.e. at β^0).

From (3.37), it is concluded that (i) the elasticity of the films acts as a corrector of the permeability and (ii) a dynamic Darcy's law slightly different from that of a material without films is obtained when $\omega_e/\omega \to 0$.

Equation (3.37) can be rewritten in the following alternative forms (see (2.47) and (2.48)) which will be used in §§ 3.3.1–3.3.3:

$$\boldsymbol{H}_s(\omega)\cdot\langle \boldsymbol{v}^{(0)}\rangle = \eta\boldsymbol{k}_s^{-1}(\omega)\left(\boldsymbol{I} + \frac{\omega_e}{\mathrm{i}\omega}\boldsymbol{B}_s(\omega)\boldsymbol{k}_s^{-1}(\omega)\right)\cdot\langle \boldsymbol{v}^{(0)}\rangle = -\boldsymbol{\nabla}_x p^{(0)}, \tag{3.38}$$

$$-\omega^2\boldsymbol{\rho}_s(\omega)\cdot\langle \boldsymbol{u}^{(0)}\rangle = -\omega^2\eta\boldsymbol{k}_s^{-1}(\omega)\left(\frac{\boldsymbol{I}}{\mathrm{i}\omega} - \frac{\omega_e}{\omega^2}\boldsymbol{B}_s(\omega)\boldsymbol{k}_s^{-1}(\omega)\right)\cdot\langle \boldsymbol{u}^{(0)}\rangle = -\boldsymbol{\nabla}_x p^{(0)}. \tag{3.39}$$

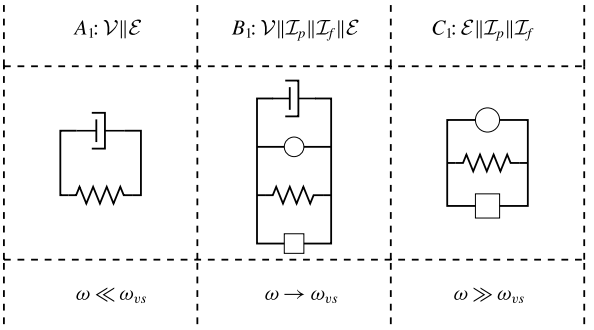

FIGURE 3. Rheological diagram representing the combination of dashpot ($\mathcal{V}$, ⊣), spring ($\mathcal{E}$, ∿) and masses ($\mathcal{I}_f$, ○ and $\mathcal{I}_p$, □) describing the acoustic behaviour of permeo-elastic materials with respect to the visco-inertial frequency ω_{vs} for the case $\omega \gg \omega_e$ (i.e. very flexible films).

For simplicity, the analysis is further conducted for an isotropic material (or for a preferential flow direction). Therefore, the tensors involved become scalar. For example, $\boldsymbol{k}_s(\omega) = \mathcal{K}_s(\omega)\boldsymbol{I}$. The analysis will be made with reference to figure 3, which shows a conceptual diagram representing the asymptotic behaviour of permeo-elastic materials with respect to the visco-inertial frequency ω_{vs} for the case $\omega \gg \omega_e$.

3.3.1. *Very flexible films – visco-elastic regime ($A_1 : \mathcal{V} \parallel \mathcal{E}$)*

For frequencies much smaller than the viscous characteristic frequency, i.e. $\omega \ll \omega_{vs} = \eta/\mathcal{K}_{s0}\varrho\alpha_\infty$, equation (3.37) becomes

$$\langle \boldsymbol{v}_i^{(0)} \rangle \cong \frac{\mathcal{K}_{s0}}{\eta}\left(1 - \frac{\omega_e}{\mathrm{i}\omega}\frac{B_{s0}}{\mathcal{K}_{s0}}\right) G_i. \tag{3.40}$$

This equation can be rewritten in the following alternative form:

$$\frac{\mu_{A_1}(\omega)}{\mathcal{K}_{s0}}\langle \boldsymbol{v}_i^{(0)} \rangle \cong G_i, \quad \text{with } \mu_{A_1}(\omega) = \eta + \frac{\omega_e \eta B_{s0}}{\mathrm{i}\omega \mathcal{K}_{s0}} = \eta + \frac{E_p}{\mathrm{i}\omega} I\theta B_{s0}\frac{\mathcal{K}_0}{\mathcal{K}_{s0}}. \tag{3.41}$$

This equation shows that the flow is characterised by (i) the permeability of the pore space including very flexible films, $\mathcal{K}_{s0}$, and (ii) a saturating effective fluid that behaves rheologically as a Kelvin–Voigt visco-elastic fluid (Boutin & Auriault 1990) with parameter $\mu_{A_1}(\omega)$. This parameter corresponds to a dashpot of viscosity η connected in parallel to a soft spring $E_K = \omega_e \eta B_{s0}/\mathcal{K}_{s0} = O(E_p I/h^3)$. The combination of elements in parallel is consistent with the fact that the fluid is forcing the deformation of the soft films. This behaviour, which is represented by A_1 (i.e. $\mathcal{V} \parallel \mathcal{E}$) in figure 3, can be alternatively seen by rewriting (3.41) as

$$\left(R_{A_1} + \frac{k_{A_1}}{\mathrm{i}\omega}\right)\langle \boldsymbol{v}_i^{(0)} \rangle = \left(\frac{\eta}{\mathcal{K}_{s0}} + \frac{1}{\mathrm{i}\omega}\frac{\omega_e \eta B_{s0}}{\mathcal{K}_{s0}^2}\right)\langle \boldsymbol{v}_i^{(0)} \rangle \cong G_i, \tag{3.42}$$

where the viscous and elastic effects are represented by $R_{A_1} = \eta/\mathcal{K}_{s0}$ and $k_{A_1} = \omega_e \eta B_{s0}/\mathcal{K}_{s0}^2$ respectively.

Recalling that $\omega \gg \omega_e$, $\omega \ll \omega_{vs}$ and $H_{s0} = \eta/\mathcal{K}_{s0}$, the effective dynamic flow resistivity and apparent dynamic density are given by

$$H_{A_1}(\omega) \cong H_{s0} + \frac{H_{s0}}{\mathrm{i}\omega}\omega_e \frac{B_{s0}}{\mathcal{K}_{s0}}, \tag{3.43}$$

$$\rho_{A_1}(\omega) \cong -\frac{H_{s0}}{\omega^2}\omega_e \frac{B_{s0}}{\mathcal{K}_{s0}} + \frac{H_{s0}}{\mathrm{i}\omega}. \tag{3.44}$$

These expressions show that the imaginary (respectively real) part of the effective dynamic flow resistivity (respectively apparent dynamic density) takes negative values. When considering the positive convention $\mathrm{e}^{\mathrm{i}\omega t}$, as in this work, such a behaviour does not exist in conventional porous materials.

3.3.2. *Very flexible films – visco-elasto-inertial regime ($B_1 : \mathcal{V} \parallel \mathcal{I}_p \parallel \mathcal{I}_f \parallel \mathcal{E}$)*

When the fluid flow enters into the visco-inertial regime, i.e. $\omega < \omega_{vs}$, and recalling that $\omega \gg \omega_e$, (3.37) takes the following form:

$$\langle \boldsymbol{v}_i^{(0)} \rangle \cong \frac{\mathcal{K}_{s0}}{\eta}\left(1 - \frac{\mathrm{i}\omega}{\omega_{vs}}\frac{\alpha_{s0}}{\alpha_\infty} - \frac{\omega_e}{\mathrm{i}\omega}\frac{B_{s0}}{\mathcal{K}_{s0}}\right) G_i, \tag{3.45}$$

which can be rewritten in the following alternative form:

$$\left(R_{B_1} + \mathrm{i}\omega(m_{B_1} + M_{B_1}) + \frac{k_{B_1}}{\mathrm{i}\omega}\right)\langle \boldsymbol{v}_i^{(0)} \rangle = \left(\frac{\eta}{\mathcal{K}_{s0}} + \mathrm{i}\omega\left(\rho_0\alpha_{s0} + \rho_p\alpha_{s0}\frac{t\Gamma_p}{\Omega_f}\right) + \frac{1}{\mathrm{i}\omega}\frac{\omega_e \eta B_{s0}}{\mathcal{K}_{s0}^2}\right)\langle \boldsymbol{v}_i^{(0)} \rangle \cong G_i. \tag{3.46}$$

It is then concluded that the fluid–film system behaves as a parallel dashpot–spring–double-mass system, as represented by B_1 (i.e. $\mathcal{V} \parallel \mathcal{I}_p \parallel \mathcal{I}_f \parallel \mathcal{E}$) in figure 3. The parameters of the system are $R_{B_1} = R_{A_1}$, $m_{B_1} = \rho_0\alpha_{s0}$, $M_{B_1} = \rho_p\alpha_{s0}t\Gamma_p/\Omega_f$, and $k_{B_1} = k_{A_1}$.

The effective dynamic flow resistivity and apparent dynamic density are given by

$$H_{B_1}(\omega) \cong H_{s0} + \frac{\mathrm{i}\omega}{\omega_{vs}}H_{s0}\frac{\alpha_{0s}}{\alpha_\infty}\left(1 - \frac{\omega_e\omega_{vs}}{\omega^2}\frac{\alpha_\infty}{\alpha_{0s}}\frac{B_{s0}}{\mathcal{K}_{s0}}\right), \tag{3.47}$$

$$\rho_{B_1}(\omega) \cong \frac{H_{s0}}{\omega_{vs}}\frac{\alpha_{0s}}{\alpha_\infty}\left(1 - \frac{\omega_e\omega_{vs}}{\omega^2}\frac{\alpha_\infty}{\alpha_{0s}}\frac{B_{s0}}{\mathcal{K}_{s0}}\right) + \frac{H_{s0}}{\mathrm{i}\omega}. \tag{3.48}$$

This equation describes the richest asymptotic behaviour of permeo-elastic media, i.e. the one in which viscous, elastic and inertial effects are involved. It reduces to (3.44) when the inertia of the fluid–film system is negligible in comparison to the elasticity of the films and predicts that the real part of the apparent dynamic density becomes null when $\omega = \sqrt{k_{B_1}/(m_{B_1} + M_{B_1})}$.

3.3.3. *Very flexible films – elasto-inertial regime ($C_1 : \mathcal{E} \parallel \mathcal{I}_p \parallel \mathcal{I}_f$)*

Neglecting viscosity effects (i.e. $\omega \gg \omega_{vs}$) and recalling that $\omega \gg \omega_e$, equation (3.37) becomes

$$\langle \boldsymbol{v}_i^{(0)} \rangle \cong \frac{\mathcal{K}_{s\infty}}{\eta}\left(1 - \frac{\omega_e}{\mathrm{i}\omega}\frac{B_{s\infty}}{\mathcal{K}_{s\infty}}\right) G_i. \tag{3.49}$$

Substitution of the values of $\mathcal{K}_{s\infty} = \mathcal{K}_{s0}\omega_{vs}/\mathrm{i}\omega$ and $B_{s\infty}$ (C 13) leads to

$$\left(\mathrm{i}\omega(m_{C_1} + M_{C_1}) + \frac{k_{C_1}}{\mathrm{i}\omega}\right)\langle \boldsymbol{v}_i^{(0)}\rangle = \left(\mathrm{i}\omega\left(\rho_0\alpha_\infty + \rho_p t\frac{\Gamma_p}{\Omega_f}\alpha_\infty\right) + \frac{E_p I\theta_g}{\mathrm{i}\omega}\right)\langle \boldsymbol{v}_i^{(0)}\rangle \cong G_i. \tag{3.50}$$

This equation shows that the fluid–film system behaves as a spring $k_{C_1} = E_p I\theta_g$ connected in parallel to the effective mass of the fluid and the films $m = m_{C_1} + M_{C_1} = \varrho\alpha_\infty$. These two masses are also connected in parallel and are given by $m_{C_1} = \rho_0\alpha_\infty$ and $M_{C_1} = \alpha_\infty\rho_p t\Gamma_p/\Omega_f = O(\alpha_\infty\rho_p t/h)$. This regime is represented by C_1 (i.e. $\mathcal{E} \parallel \mathcal{I}_p \parallel \mathcal{I}_f$) in figure 3.

The effective dynamic flow resistivity and apparent dynamic density are given by

$$H_{C_1}(\omega) \cong \mathrm{i}\omega\frac{H_{s0}}{\omega_{vs}}\left(1 - \frac{\omega_g^2}{\omega^2}\right), \tag{3.51}$$

$$\rho_{C_1}(\omega) \cong \frac{H_{s0}}{\omega_{vs}}\left(1 - \frac{\omega_g^2}{\omega^2}\right). \tag{3.52}$$

This equation shows that the apparent dynamic density becomes null at $\omega = \omega_g$, while the effective permeability tends to infinity. This is a typical resonance effect observed in an elasto-inertial system and appears as a macroscopic consequence of the fluid–film interaction at the pore scale. It is worth noting that in the elasto-inertial regime and for $\omega < \omega_g$, an overlap of the fluid–film system response given by (3.34) and (3.50) is predicted. In such a case, the effective permeability can be estimated by considering the leading-order term in (3.34) (i.e. the behaviour is inertia-dominated) and both terms in (3.50) as $\mathcal{K}(\omega) \cong \eta\left(1/\mathrm{i}\omega m_{c_1} + 1/(\mathrm{i}\omega(m_{C_1} + M_{C_1}) + k_{C_1}/\mathrm{i}\omega)\right)^{-1}$. Further algebra leads us to obtain that the effective permeability becomes null at $\omega^2 = \omega_g^2/(1 + \rho_0\alpha'_\infty/\varrho\alpha_\infty)$, with $\alpha'_\infty = \alpha_{\infty r}$, which further justifies the estimation of ω_0 given by (3.15).

As a final remark, it should be mentioned that for frequencies $\omega \gg \omega_g$, the elastic effects become negligible and the fluid–film system behaviour is determined solely by the inertia of the fluid and the films. Hence, one has that $\rho(\omega) = \varrho\alpha_\infty$ (see also § 3.1.1).

4. Examples and experimental validation

4.1. *Illustrating examples*

This section illustrates the theoretical results obtained in the previous sections for permeo-elastic media. We consider an air-saturated material made of a solid matrix with an embedded array of cylindrical pores into which periodically distributed coaxial short tubes are inserted. The films are fixed on one of the extremes of the short tubes, while the other extremes are open. The geometry of the material is shown in figure 4, together with a 2D axisymmetric geometry of one cylindrical pore with the inserted short tubes with films and the unit cell. We emphasise that the physics of the array is mostly captured by the phenomena occurring in the tubes. The radius of the cylindrical pore is represented by r_0, while the short tube inner radius and length are represented by r_c and t_c respectively. The size of the gap formed in between the tube and the walls of the cylindrical pore is denoted as g, while the thickness of the tube walls is given by $w = r_0 - r_c - g$. The unit cell of the material has a length t_0 and the distance between the short tubes is $t_0 - t_c$.

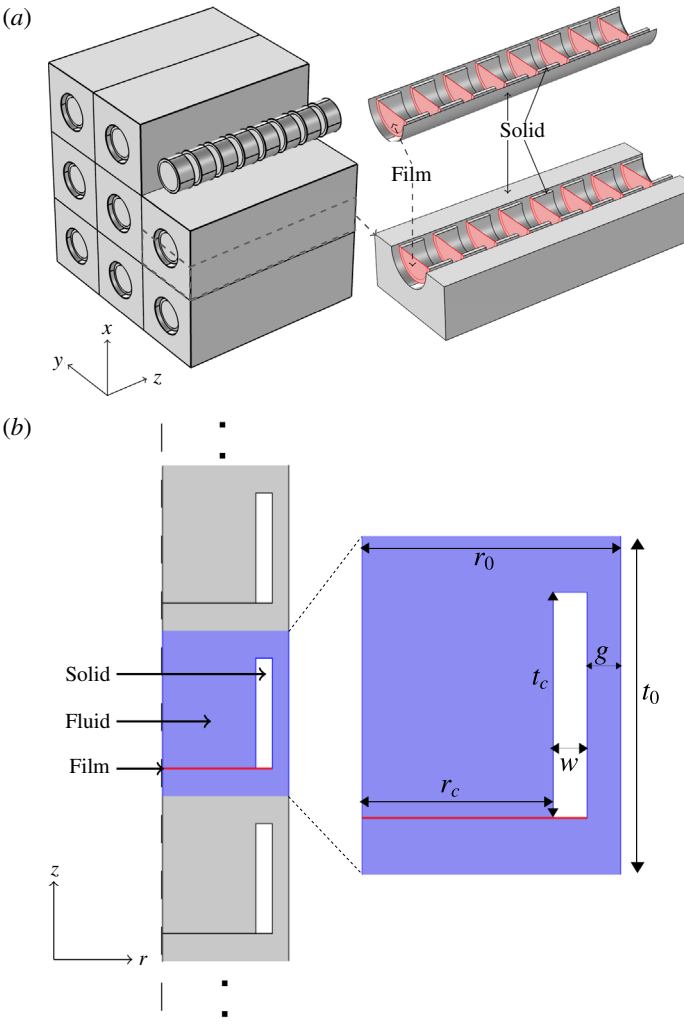

FIGURE 4. (Colour online) (*a*) Array of cylindrical pores with periodically distributed coaxial short tubes with clamped films on one of their extremes (left) and section views (right). (*b*) Two-dimensional axisymmetric geometry of a cylindrical pore with the inserted short tubes with films (left) and geometrical parameters of the unit cell of the material (right).

The mechanical parameters of a polyetherimide (PEI) film sample are considered as reference. These are $\rho_p = 1200$ kg m^{-3}, $\nu = 0.36$, $t = 75$ μm and $E = E_0 = 6.9$ GPa. To illustrate the properties of the materials, we first consider the following geometrical parameters: $r_g = 23$ mm, $r_c = 17$ mm, $t_c = 20$ mm, $w = 3$ mm and $t_0 = 30$ mm, which result in a porosity of $\phi = 0.86$. It should be noted that this porosity corresponds to that of one cylindrical pore with the inserted short tubes.

If one considers two extreme values of the Young's modulus, $E \to 0$ and $E \to \infty$, corresponding approximately to the cases of materials without films and with perfectly rigid films, the permeabilities and tortuosities are given by $(2.46 \times 10^{-5};\ 2.3 \times 10^{-7})$ m^2 and $(1.03;\ 3.16)$ respectively. One can then conclude

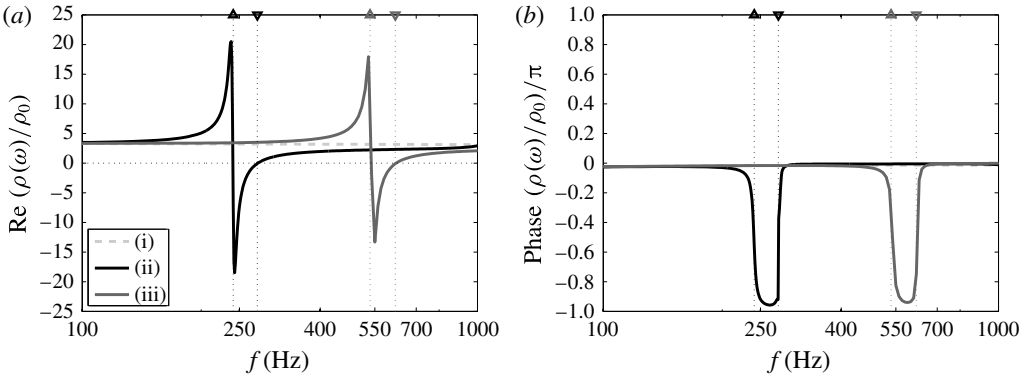

FIGURE 5. Real part (a) and phase (b) of the normalised apparent dynamic density $\rho(\omega)/\rho_0$ of a material with perfectly rigid films (i), and permeo-elastic materials with $E = E_0$ (ii) and $E = 5E_0$ (iii). The vertical dotted lines with downward- and upward-pointing triangles represent $f_0 = \omega_0/2\pi$ and $f_g = \omega_g/2\pi$ respectively.

that very different acoustical properties can be observed when varying the elastic properties of the films. In addition, it is further noticed that (i) the material with perfectly rigid films will be dominated by inertial effects in the audible frequency range since the Biot frequency is 2.85 Hz and (ii) the in-vacuum fundamental resonance frequency of the clamped films is 313 Hz.

In the remaining part of this section, we will present the results for two quantities that are normally used in the field of acoustics of porous media (Allard & Atalla 2009), namely the apparent dynamic density and the speed of sound.

Figure 5 shows the real part and phase of the apparent dynamic density of a permeo-elastic material compared with those of a material with perfectly rigid films. This effective parameter has been calculated for an infinite array of short tubes with films from the solution of the fluid–structure interaction problem (2.24)–(2.31) in a 2D axisymmetric unit cell (see figure 4). The solution was obtained numerically using the finite element method and the software COMSOL Multiphysics® (COMSOL 2013). In particular, an arbitrary Lagrangian–Eulerian formulation implemented in this software was used and a fully coupled solver (MUMPS) that involves the simultaneous solution of the fields was considered. Lagrangian linear elements modelled the fluid velocity and pressure (i.e. a P1–P1 formulation with streamline diffusion as stabilisation method), while quadratic elements approximated the film displacement. A triangular mesh in combination with a layered quadrilateral mesh to resolve the boundary layers was used. Furthermore, the mesh coincided on the periodic boundaries of the unit cell and a mesh refining analysis was conducted to ensure the convergence of the solution.

As discussed in § 3.2.3, the films behave as quasi-rigid at low frequencies. Hence, the real part of the apparent dynamic density and its phase approach those of a material with perfectly rigid films. As the frequency increases, this behaviour overlaps with that described in § 3.3.3 and the fluid–film system enters into the resonance zone. The frequency at which the apparent dynamic density tends theoretically to infinity is $f_0 = 241$ Hz. The fundamental resonance frequency of the fluid–film system with $E = E_0$ is $f_g = 277$ Hz. This is smaller than the in-vacuum fundamental resonance frequency due to the fluid loading on the films (see Filippi 2008, Ch. 3). In between the two elasto-inertial frequencies f_0 and f_g, an atypical band is observed where the

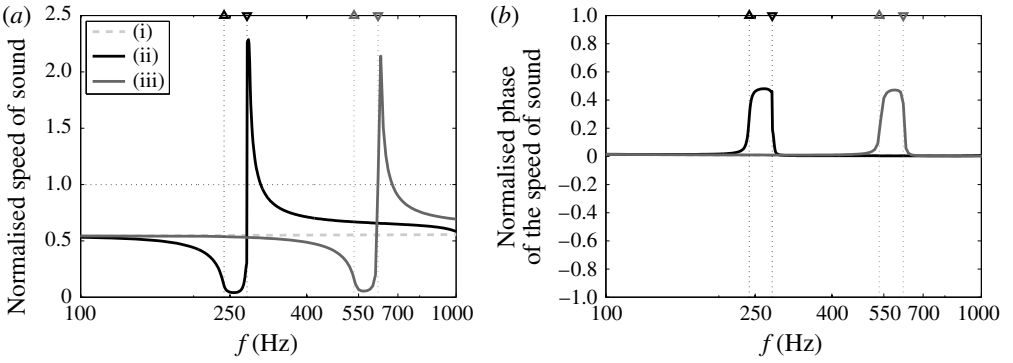

FIGURE 6. (*a*) Real part of the normalised speed of sound $\mathrm{Re}(\mathcal{C}(\omega)/c_0)$. (*b*) Normalised phase of the normalised speed of sound $\mathrm{Phase}(\mathcal{C}(\omega)/c_0)/\pi$. Material with perfectly rigid films (i), and permeo-elastic material with $E = E_0$ (ii) and $E = 5E_0$ (iii). The vertical dotted lines with downward- and upward-pointing triangles represent f_0 and f_g respectively.

real part of the apparent dynamic density becomes negative and its phase tends to $-\pi$. In the atypical band, the fluid movement is opposite in phase with respect to the carrying wave outside the inner resonating units. As a consequence, the average movement leads to a negative apparent density with an unusual phase value. Such a behaviour is a direct consequence of the fluid–film interaction at the pore scale and does not exist in conventional porous materials. In the latter type of material, the real part of the apparent dynamic density is always positive and its phase varies in between its values for viscous and inertial fluid flow, i.e. from $-\pi/2$ to 0 (Johnson, Koplik & Dashen 1987; Smeulders, Eggels & van Dongen 1992). As predicted by (3.10), the fundamental resonance frequency for the same material but with films with elastic modulus $E = 5E_0$ is increased by a factor of approximately $\sqrt{5}$, i.e. $f_g = 621$ Hz, with respect to that of the material with $E = E_0$. In turn, the frequency f_0 is also increased by the same factor.

Figure 6 shows the real part and phase of the normalised speed of sound in the material. It should be noted that to calculate this, the bulk modulus (2.51) was calculated using the following semi-phenomenological model (Lafarge *et al.* 1997): $K(\omega) = P_0/(1 - j\omega F(\omega)(\gamma - 1)/\gamma\omega_t)$, with $F(\omega) = 1/(j\omega/\omega_t + \sqrt{1 + j\omega M_t/2\omega_t})$. Here, $\omega_t = \kappa/\rho_0 C_p k_0'$ is the thermal characteristic frequency, $M_t = 8k_0'/\Lambda'^2$ is the thermal shape factor, $\kappa/\rho_0 C_p$ is the thermal diffusivity, $\Lambda' = 2|\Omega_f|/(|\Gamma_s| + |\Gamma_p|)$ is the thermal characteristic length and k_0' is the static thermal permeability. The latter has been numerically calculated by spatially averaging the solution of a static heat conduction problem with respect to the fluid phase, as detailed, for example, in Venegas & Umnova (2011). At low frequencies, the speed of sound of permeo-elastic materials tends to that of a material with perfectly rigid films. A significant decrease in speed of sound is observed in the atypical band. Moreover, the phase of the speed of sound in this band tends to $\pi/2$, i.e. the waves are overdamped. At the fundamental resonance frequency, and for slightly higher frequencies, supersonic velocities are observed. In conventional porous materials, the phase of the speed of sound varies from $\pi/4$ to 0 and the real part of the speed of sound is bounded by its inertial value, i.e. by the speed of sound in the saturating fluid c_0 divided by the square root of the tortuosity. It is clear that the acoustic behaviour of permeo-elastic materials is significantly different.

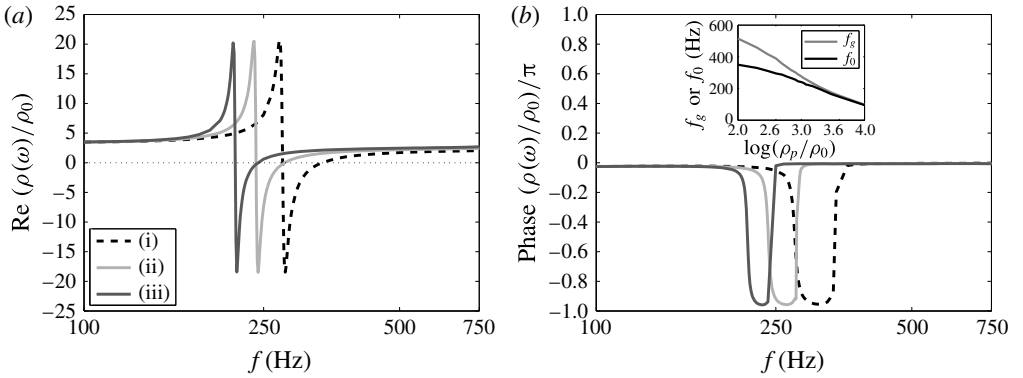

FIGURE 7. Real part (*a*) and phase (*b*) of the normalised apparent dynamic density $\rho(\omega)/\rho_0$ of a material with film density $\rho_p = 0.6\rho_{p0}$ (i.e. $\varrho = 2.785$ kg m^{-3}) (i), $\rho_p = \rho_{p0}$ (i.e. $\varrho = 3.839$ kg m^{-3}) (ii) and $\rho_p = 1.4\rho_{p0}$ (i.e. $\varrho = 4.894$ kg m^{-3}) (iii), with $\rho_{p0} = 1200$ kg m^{-3}. The inset plot shows the elasto-inertial characteristic frequencies f_g (grey line) and f_0 (black line) as a function of the ratio between the film density and the saturating fluid density ($\rho_0 = 1.204$ kg m^{-3}).

Figure 7 shows the influence of the density of the films on the real part and phase of the normalised apparent dynamic density. Heavier films provide smaller elasto-inertial characteristic frequencies. However, the behaviour is qualitatively similar to that obtained when varying the elastic modulus of the films. As predicted by (3.15), the elasto-inertial frequencies f_g and f_0 become closer to each other as the density of the films is increased. This is shown in the inset plot of figure 7, where f_g and f_0 are plotted as a function of the ratio between the densities of the films and the saturating fluid. The net effect is that the atypical band where the apparent dynamic density becomes negative and its phase shows unusual values becomes much narrower as the density ratio increases. Hence, lightweight films, i.e. $O(\varrho) = O(\rho_0)$, are preferred to observe permeo-elastic effects.

The influence of viscous dissipation on the apparent dynamic density of permeo-elastic materials has been assessed by decreasing the size of the gap g formed in between the short tubes and the cylindrical pore wall (see figure 4). The results are shown in figure 8. The other geometrical and mechanical parameters (with $E = E_0$) are the same as those in figure 5. The static permeability is decreased when the gap size becomes smaller. For example, this parameter for the material with the narrowest gap ($g = 0.4$ mm) is of the order of 290 times smaller than that with the widest gap ($g = 3$ mm). This results in a higher (respectively lower) visco-inertial (respectively visco-elastic) characteristic frequency. It should be noted, however, that the fundamental resonance frequency f_g remains constant. The behaviour of the fluid–film system at low frequencies is determined by the low-frequency inertia of the fluid that is affected by the elasticity of the films, as developed in § 3.2.2. As the frequency increases, the behaviour overlaps with that described in § 3.3.2. This means that the fluid flow regime in the fluid–film system is influenced by viscosity, elasticity and the inertia of the fluid and the films. Then, the fluid–film system enters into the elasto-inertial regime described in § 3.3.3. An increase in the effects of viscosity leads to an increase of the bandwidth of the atypical band. For example, the atypical band covers frequency regions of $B \approx 277 - 197 = 80$ Hz and $B \approx 277 - 87 = 190$ Hz when $g = 1$ mm and $g = 0.4$ mm respectively. Furthermore, the peak associated with

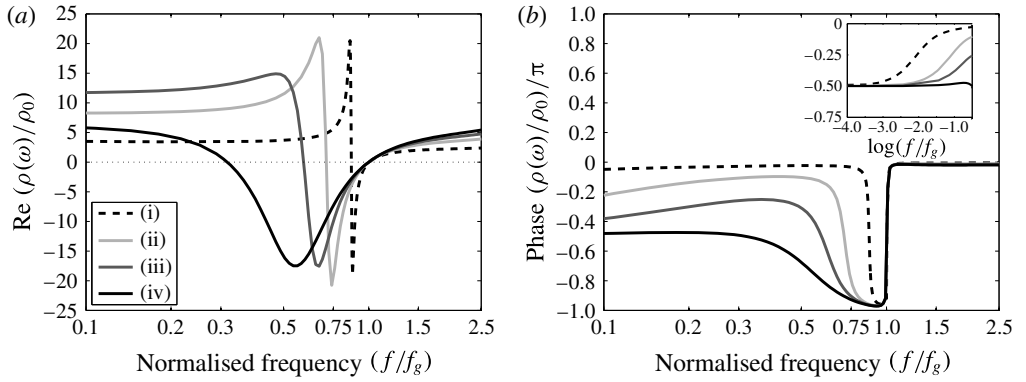

FIGURE 8. Influence of viscosity effects on the real part (*a*) and phase (*b*) of the normalised apparent dynamic density $\rho(\omega)/\rho_0$: (i) $g = 3$ mm, (ii) $g = 1$ mm, (iii) $g = 0.6$ mm, (iv) $g = 0.4$ mm. The inset plot shows the values of the phase of $\rho(\omega)/\rho_0$ at lower frequencies. The frequency has been normalised to $f_g = 277$ Hz.

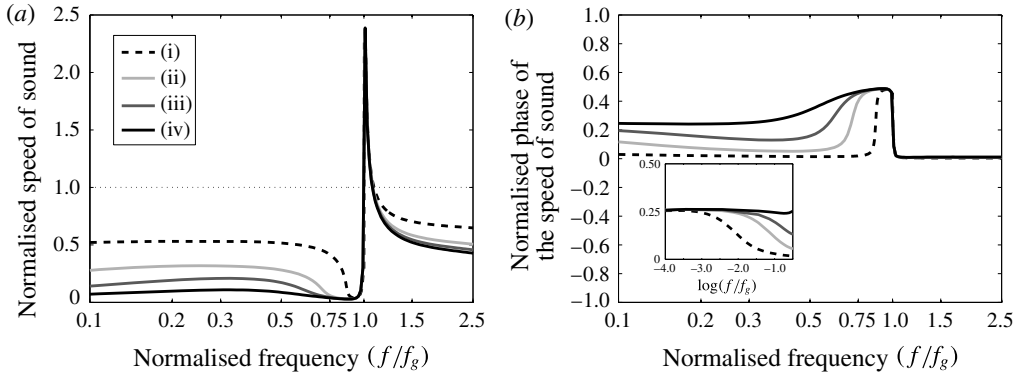

FIGURE 9. Influence of viscosity effects on the real part of the normalised speed of sound $\mathrm{Re}(\mathcal{C}(\omega)/c_0)$ (*a*) and the normalised phase of the normalised speed of sound $\mathrm{Phase}(\mathcal{C}(\omega)/c_0)/\pi$ (*b*) for permeo-elastic materials with (i) $g = 3$ mm, (ii) $g = 1$ mm, (iii) $g = 0.6$ mm and (iv) $g = 0.4$ mm. The inset plot shows the normalised phase of the normalised speed of sound at lower frequencies. The frequency has been normalised to $f_g = 277$ Hz.

f_0 decreases in amplitude until it becomes highly damped and no longer appears. The latter occurs when the visco-inertial frequency approaches f_g. On the other hand, the wider atypical band leads to a wider frequency region where the sound waves are slowed down, as shown in figure 9, where the normalised speed of sound and its phase are presented. It must be emphasised that in this frequency range, the magnitude of the imaginary part of the apparent dynamic density is much larger than that of its real part, which reflects the fact that viscosity effects dominate in this frequency range. Hence, the first zero value of the real part of the apparent dynamic density in figure 8 does not induce supersonic velocities in the effective fluid–film system.

Equation (3.32) predicts that the real part of the apparent dynamic density could be either null or negative in a wide range of frequency depending on the interaction

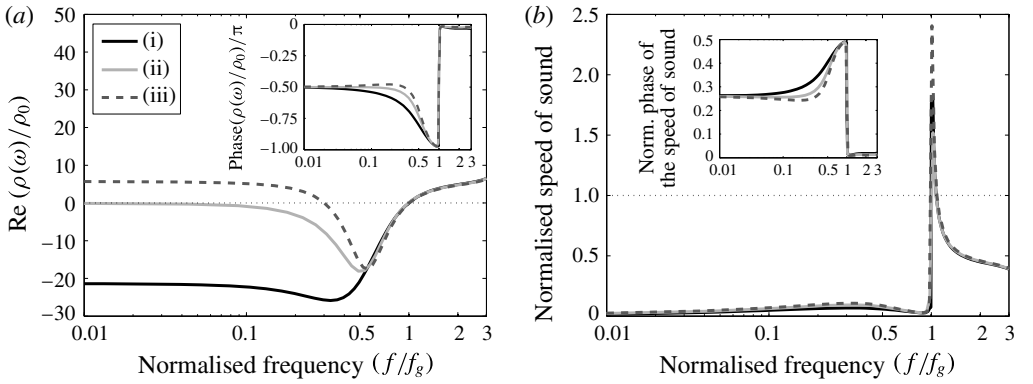

FIGURE 10. Real part of the normalised apparent dynamic density $\rho(\omega)/\rho_0$ (*a*) and speed of sound $\mathcal{C}(\omega)/c_0$ (*b*) of permeo-elastic materials with (i) $E = 0.3E_0 = 2070$ MPa, (ii) $E = 0.65E_0 = 4485$ MPa and (iii) $E = 0.95E_0 = 6555$ MPa. The inset plots show the normalised phase values. The frequency has been normalised to (i) $f_g = 152$ Hz, (ii) $f_g = 225$ Hz and (iii) $f_g = 268$ Hz.

between the low-frequency inertia of the fluid and the elasticity of the films. This is evidenced in figure 10, where the real part of the apparent dynamic density and its phase are shown for three different elastic modulus values, i.e. $E = 0.3E_0$, $E = 0.65E_0$ and $E = 0.95E_0$. The geometrical parameters are as in figure 5, except that the gap size is set to $g = 0.4$ mm. The strongest effect of the elasticity is observed for the material with the smallest Young's modulus. This shows a wide-band negative real part of the apparent dynamic density. For the material with intermediate Young's modulus value, the elastic effects compensate those due to the low-frequency inertia of the fluid. This leads to a nearly null real part of the apparent dynamic density. As previously argued, the behaviour in this frequency region is dominated by viscosity effects. Therefore, the nearly null real part of the apparent dynamic density does not lead to supersonic velocities in the fluid–film system, as can be seen in the plot in figure 10(*b*).

4.2. *Experimental validation*

This section presents results of experiments conducted on a single unit cell of a prototype permeo-elastic material corresponding to that illustrated by figure 4(*b*) (right). Since the physics of a periodic array is mostly determined by that in a unit cell, our experimental work focuses on measuring the acoustical properties of a single unit cell. This allows us to study the most relevant features of permeo-elastic materials.

For convenience, measurements of surface impedance have been taken in an impedance tube by following the procedure described in ISO 10534-2:2001 (2001). A diagram of the measurement set-up is presented in figure 11. The measured magnitude and phase of the surface impedance $Z_w(\omega)$ normalised to the characteristic impedance of the saturating fluid, $Z_0 = \rho_0 c_0$, are shown in figure 12. These measurements have been taken on a configuration composed of an air gap backed by a single unit cell of the permeo-elastic material, which is backed by a rigidly backed plenum, as illustrated in figure 11. The film material is PEI, whose parameters are $E = E_0 = 6.9$ GPa, $\rho_p = 1200$ kg m^{-3}, $\nu = 0.36$ and $t = 75$ μm. The other parameters of the geometry can be inferred from figure 11.

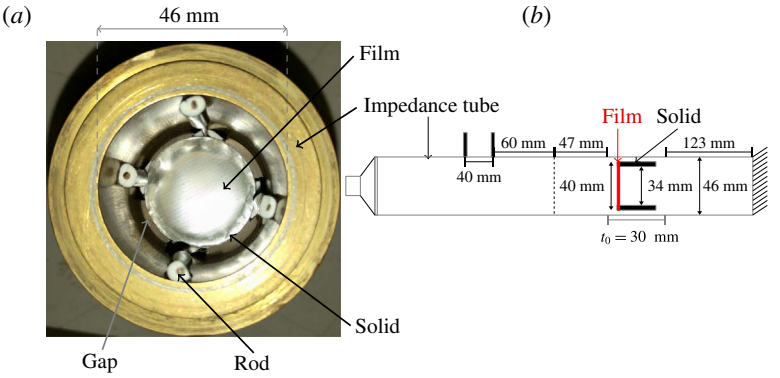

FIGURE 11. (Colour online) (*a*) Unit cell of the prototype permeo-elastic material placed in the impedance tube. (*b*) Diagram of the impedance tube used to measure the surface impedance of a prototype permeo-elastic material. The vertical dashed line represents the front surface of the measured configuration.

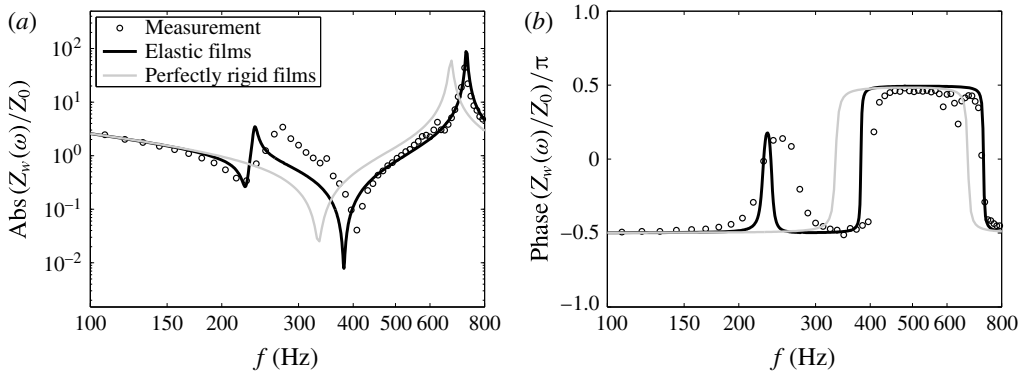

FIGURE 12. Measured and predicted normalised magnitude (*a*) and phase (*b*) of the surface impedance of a permeo-elastic material and a material with perfectly rigid films.

The validation of the theory is conducted by comparing the measured experimental data with numerical calculations of surface impedance. The latter was calculated as follows. The dynamic permeability was numerically calculated for an infinite array from the solution of the fluid–film interaction problem (2.24)–(2.31), while the bulk modulus was calculated using the semi-phenomenological model proposed in Lafarge *et al.* (1997), whose input parameters were also obtained numerically as detailed above. This parameter and the apparent dynamic density were used to calculate the wavenumber and characteristic impedance using (2.51). Then, a transfer matrix approach (Allard & Atalla 2009) was used to take into account the air gaps in front of and behind the prototype material (see figure 11).

The predictions of the model shown in figure 12 and the measured values are in reasonable agreement. The developed theory explains and the numerical model captures the local peak of the magnitude of the surface impedance as well as the change in phase around the atypical band where the apparent dynamic density takes negative values. This phenomenon does not exist in the material with perfectly rigid films.

The discrepancies between the numerical and experimental results, i.e. prediction of a narrower band where the phase is shifted and the local peak in the magnitude of the surface impedance being located at a slightly lower frequency, may be due to the following factors. (i) The effective parameters have been determined for an infinite array, while only one period has been measured. This means that, in principle, the theoretical model cannot exactly reproduce the conditions of the prototype material used in the experiment. (ii) The internal damping of the elastic films has not been accounted for. Similarly to viscosity effects, this could lead to a wider atypical band. (iii) The mounting rods used to build the prototype material (see figure 11) are not considered in the 2D axisymmetric numerical model. These rods decrease the effective gap size in between the short tube and the wall of the impedance tube. This smaller gap can lead to a larger influence of viscosity effects which may result in an increase of the bandwidth of the atypical band, as shown in figure 8. (iv) The practical implementation of the perfect clamping condition of the films may not be accurate. This could lead to a variation in the eigenfrequency values.

5. Conclusions

This paper investigated the effective dynamic properties of permeo-elastic materials using the two-scale asymptotic homogenisation method. This class of material possesses a specific solid frame architecture: the microstructure is composed of a stiff skeleton onto which flexible films are fixed. In contrast to the classical case of Biot poroelastic materials, where the fluid flow is not affected by the deformation of the solid frame, the films are deformed by the fluid flow. Due to this fluid–film interaction, the notion of dynamic permeability determined in an undeformed frame no longer applies. We have shown that accounting for the elasticity and inertia of the films leads to a non-conventional constitutive dynamic fluid flow law as opposed to the standard dynamic Darcy's law. For instance, the fluid–film system can behave as an equivalent visco-elastic fluid as well as exhibiting local resonances. Therefore, the acoustic behaviour is substantially different from that described by the standard Biot poroelastic theory, as evidenced theoretically, numerically and experimentally in this work.

We emphasise that our work was conducted within the framework of a small deformation regime and that the fluid–film interaction influences the permeability of the effective saturating fluid, while its effective compressibility remains unchanged. Hence, our work introduces new possibilities for designing or describing porous media with non-conventional features. Applications of our results may include materials for acoustical engineering (e.g. soft perforated open-cell foams), inverse methods in mechanics of soft films, and mechanics of biological materials (e.g. bio-films or cell walls).

Extensions of this work in different directions may include the study of viscoelasticity in polymeric films, which could induce a strong dependence on temperature of the fluid–film interaction, unconventional mass transport in liquid-saturated media in both permanent and dynamic regimes, and the macroscopic description of permeo-elastic media accounting for the stiffness of the solid frame.

Acknowledgements

This work has been funded by the project METAUDIBLE (ANR 13-BS09-0003-03), co-funded by the Agence Nationale de la Recherche ANR and Fondation de Recherche pour l'Aéronautique et l'Espace FRAE, and was conducted within the

framework of CeLyA of Université de Lyon operated by ANR (ANR-10-LABX-0060 and ANR-11-IDEX-0007). The authors are grateful to F. Sallet for his help in the experimental part of this work and to Dr A. Elliott for providing material samples.

Appendix A

The derivation of the variational formulation (2.33) associated with the fluid–structure interaction cell problem (2.24)–(2.31) is detailed in this appendix.

We consider the vectorial space $\mathcal{W}$ of complex velocity fields $\boldsymbol{w}$ defined in $\Omega_f \cup \Gamma_p$ such that $\boldsymbol{w}$ is Ω-periodic, divergence free $\nabla_y \cdot \boldsymbol{w} = 0$ in Ω_f, with $\boldsymbol{w} = 0$ on Γ_s, $\boldsymbol{w} = w\boldsymbol{N}$ on Γ_p, and $w = 0$ and $\nabla_{yp} w \cdot \boldsymbol{n} = 0$ on $\partial\Gamma_p$. As shown in § 2.5, $\mathcal{W}$ equipped with the norm (2.32) is a Hilbert space.

In order to derive the variational formulation (2.33), the fluid flow problem is considered first. The equation of conservation of momentum (2.24) is multiplied by the conjugate of $\boldsymbol{w}$, i.e. $\overline{\boldsymbol{w}}$, and integrated over Ω_f,

$$\int_{\Omega_f} \mathrm{div}_y(\boldsymbol{\sigma}_f^{(1)}) \cdot \overline{\boldsymbol{w}} \, \mathrm{d}\Omega = \int_{\Omega_f} \mathrm{i}\omega\rho_0 \boldsymbol{v}^{(0)} \cdot \overline{\boldsymbol{w}} \, \mathrm{d}\Omega + \int_{\Omega_f} \nabla_x p^{(0)} \cdot \overline{\boldsymbol{w}} \, \mathrm{d}\Omega. \tag{A 1}$$

Integration by parts of the left-hand side integral, application of the divergence theorem and noting that $\boldsymbol{I} : \boldsymbol{D}_y(\overline{\boldsymbol{w}}) = \nabla_y \cdot \overline{\boldsymbol{w}} = 0$ in Ω_f lead to

$$\int_{\Omega_f} \mathrm{div}_y(\boldsymbol{\sigma}_f^{(1)}) \cdot \overline{\boldsymbol{w}} \, \mathrm{d}\Omega = \int_{\partial\Omega_f} \boldsymbol{\sigma}_f^{(1)} \cdot \boldsymbol{N} \cdot \overline{\boldsymbol{w}} \, \mathrm{d}\Gamma - \int_{\Omega_f} 2\eta \boldsymbol{D}_y(\boldsymbol{v}^{(0)}) : \boldsymbol{D}_y(\overline{\boldsymbol{w}}) \, \mathrm{d}\Omega. \tag{A 2}$$

Denoting the periodic boundaries of the fluid network as Γ_f and recalling that $\partial\Omega_f = \Gamma_s \cup \Gamma_p \cup \Gamma_f$, the surface integral in (A 2), which cancels out on opposite boundaries of the cell due to periodicity and is null on Γ_s because of the zero velocity condition (2.26), becomes

$$\int_{\partial\Omega_f} \boldsymbol{\sigma}_f^{(1)} \cdot \boldsymbol{N} \cdot \overline{\boldsymbol{w}} \, \mathrm{d}\Gamma = -\int_{\Gamma_p} [\boldsymbol{\sigma}_f^{(1)} \cdot \boldsymbol{N}] \cdot \overline{w}\boldsymbol{N} \, \mathrm{d}\Gamma, \tag{A 3}$$

where $[\zeta]$ denotes the jump in ζ across the interface Γ_p. It should be emphasised that the films are considered as planes, i.e. their thicknesses are negligible.

Using (A 2)–(A 3), one can rewrite (A 1) as

$$\begin{aligned} -\int_{\Omega_f} \nabla_x p^{(0)} \cdot \overline{\boldsymbol{w}} \, \mathrm{d}\Omega \;=\; & \eta \int_{\Omega_f} 2\boldsymbol{D}_y(\boldsymbol{v}^{(0)}) : \boldsymbol{D}_y(\overline{\boldsymbol{w}}) \, \mathrm{d}\Omega + \mathrm{i}\omega\rho_0 \int_{\Omega_f} \boldsymbol{v}^{(0)} \cdot \overline{\boldsymbol{w}} \, \mathrm{d}\Omega \\ & + \int_{\Gamma_p} [\boldsymbol{\sigma}_f^{(1)} \cdot \boldsymbol{N}] \cdot \overline{w}\boldsymbol{N} \, \mathrm{d}\Gamma. \end{aligned} \tag{A 4}$$

This equation represents the classical variational formulation of the forced Stokes problem except that the surface integral accounts for the fluid–film interaction. This surface integral can be further developed as follows.

The momentum balance of the films (2.28) is multiplied by $\overline{w}$ and integrated over Γ_p, i.e.

$$\int_{\Gamma_p} [\boldsymbol{\sigma}_f^{(1)} \cdot \boldsymbol{N}] \cdot \overline{w}\boldsymbol{N} \, \mathrm{d}\Gamma = -\int_{\Gamma_p} \nabla_{yp} \cdot \boldsymbol{T}^{(0)} \overline{w} \, \mathrm{d}\Gamma - \rho_p t\omega^2 \int_{\Gamma_p} u^{(0)} \overline{w} \, \mathrm{d}\Gamma. \tag{A 5}$$

Integration by parts and application of the divergence theorem lead to

$$\int_{\Gamma_p} \nabla_{yp} \cdot \boldsymbol{T}^{(0)} \overline{w} \, \mathrm{d}\Gamma = \int_{\partial\Gamma_p} \boldsymbol{T}^{(0)} \cdot \overline{w} \boldsymbol{n} ds - \int_{\Gamma_p} \boldsymbol{T}^{(0)} \cdot \nabla_{yp} \overline{w} \, \mathrm{d}\Gamma. \tag{A 6}$$

The first integral on the right-hand side is null because the films are clamped, i.e. $w = 0$ on $\partial\Gamma_p$. Substitution of the moment balance (2.29) into (A 6) yields

$$\int_{\Gamma_p} \nabla_{yp} \cdot \boldsymbol{T}^{(0)} \overline{w} \, \mathrm{d}\Gamma = \int_{\Gamma_p} \mathrm{div}_{yp}(\boldsymbol{M}^{(0)}) \cdot \nabla_{yp} \overline{w} \, \mathrm{d}\Gamma. \tag{A 7}$$

By integrating by parts, applying the divergence theorem and considering the symmetry of $\boldsymbol{M}^{(0)}$, one obtains

$$\int_{\Gamma_p} \nabla_{yp} \cdot \boldsymbol{T}^{(0)} \overline{w} \, \mathrm{d}\Gamma = + \int_{\partial\Gamma_p} (\boldsymbol{M}^{(0)} \cdot \nabla_{yp} \overline{w}) \cdot \boldsymbol{n} \, \mathrm{d}s - \int_{\Gamma_p} \boldsymbol{M}^{(0)} : \boldsymbol{e}_p(\nabla_{yp} \overline{w}) \, \mathrm{d}\Gamma. \tag{A 8}$$

Since the films are clamped, i.e. $\nabla_{yp} w \cdot \boldsymbol{n} = 0$ on $\partial\Gamma_p$, the first integral on the right-hand side vanishes. On substituting the constitutive law of the films (2.30) into (A 8) and noting that $\boldsymbol{I} : \boldsymbol{e}_p(\nabla_{yp} \overline{w}) = \Delta_{yp} \overline{w}$, one obtains

$$\int_{\Gamma_p} \nabla_{yp} \cdot \boldsymbol{T}^{(0)} \overline{w} \, \mathrm{d}\Gamma = -E_p I \int_{\Gamma_p} \mathcal{N}(u^{(0)}, w) \, \mathrm{d}\Gamma. \tag{A 9}$$

Substitution of this expression into (A 5) yields

$$\int_{\Gamma_p} [\boldsymbol{\sigma}_f^{(1)} \cdot \boldsymbol{N}] \cdot \overline{w} \boldsymbol{N} \, \mathrm{d}\Gamma = -\rho_p t \omega^2 \int_{\Gamma_p} u^{(0)} \overline{w} \, \mathrm{d}\Gamma + E_p I \int_{\Gamma_p} \mathcal{N}(u^{(0)}, w) \, \mathrm{d}\Gamma. \tag{A 10}$$

Finally, the variational formulation (2.33) is obtained by substituting (A 10) into (A 4).

Appendix B

The cell problem (2.24)–(2.31) is analysed in this appendix for the limiting case of very rigid films, i.e. $E_p I \to \infty$, or low frequencies, as will become apparent below. The cell problem is rewritten in terms of the visco-elastic characteristic frequency ω_e as

$$\mathrm{div}_y(\boldsymbol{\sigma}_f^{(1)}) = \mathrm{i}\omega\rho_0 \boldsymbol{v}^{(0)} + \nabla_x p^{(0)} \quad \text{in } \Omega_f, \tag{B 1}$$

$$\nabla_y \cdot \boldsymbol{v}^{(0)} = 0 \quad \text{in } \Omega_f, \tag{B 2}$$

$$\boldsymbol{v}^{(0)} = v^{(0)} \boldsymbol{N} \quad \text{on } \Gamma_p, \quad \boldsymbol{v}^{(0)} = \boldsymbol{0} \quad \text{on } \Gamma_s, \tag{B 3a,b}$$

$$-\frac{\omega_e}{\mathrm{i}\omega} \frac{\eta}{\mathcal{K}_0 \theta} \nabla_{yp} \cdot (\mathrm{div}_{yp}(\mathcal{M}(v^{(0)}))) = \mathrm{i}\omega\rho_p t v^{(0)} - [\boldsymbol{\sigma}_f^{(1)} \cdot \boldsymbol{N}] \cdot \boldsymbol{N} \quad \text{on } \Gamma_p, \tag{B 4}$$

$$v^{(0)} = 0 \quad \text{and} \quad \nabla_{yp} v^{(0)} \cdot \boldsymbol{n} = 0 \quad \text{on } \partial\Gamma_p. \tag{B 5a,b}$$

A small parameter $\alpha = \mathrm{i}\omega/\omega_e$ is identified in (B 4). It is clear that $\alpha \to 0$ when $\omega \ll \omega_e$. This condition is satisfied when either $E_p I \to \infty$ (rigid films) or $\omega \to 0$. The variables are then looked for as expansion series of the type $\boldsymbol{v}^{(0)} = \sum_{i=0}^{\infty} \alpha^i \boldsymbol{v}^{[i]}$, $\boldsymbol{\sigma}_f^{(1)} = \sum_{i=0}^{\infty} \alpha^i \boldsymbol{\sigma}_f^{[i]}$ and $v^{(0)} = \sum_{i=0}^{\infty} \alpha^i v^{[i]}$. After substituting these series into the set

(B 1)–(B 5) and identifying the terms in powers of α, one obtains at α^{-1} that the velocity of the films is governed by

$$\nabla_{yp} \cdot (\mathrm{div}_{yp}(\mathcal{M}(v^{[0]}))) = 0 \quad \text{on } \Gamma_p, \tag{B 6}$$

$$v^{[0]} = 0 \quad \text{and} \quad \nabla_{yp} v^{[0]} \cdot \boldsymbol{n} = 0 \quad \text{on } \partial\Gamma_p. \tag{B 7a,b}$$

This leads to $v^{[0]} = 0$, which means that the films are motionless at the leading order. In turn, the fluid flow at the leading order is governed by the oscillatory Stokes problem (i.e. (B 1)–(B 3), with $\boldsymbol{v}^{[0]} = 0$ on Γ_p) in a pore space geometry with perfectly rigid films. Its solution is given by

$$\boldsymbol{v}^{[0]} = -\frac{\widehat{\boldsymbol{k}}_r(y, \omega)}{\eta} \cdot \nabla_x p^{(0)}, \tag{B 8}$$

$$p^{[0]} = -\widehat{\pi}^{[0]}(y, \omega) \cdot \nabla_x p^{(0)} + \widehat{p}^{[0]}, \tag{B 9}$$

where $\widehat{\boldsymbol{k}}_r(y, \omega)$ represents the Ω-periodic local field of velocity, and the pressure field has been expressed in terms of its zero mean part $\widehat{\pi}^{[0]}(y, \omega)$ and an integration constant $\widehat{p}^{[0]}$.

Further identification leads to the following problem for the velocity of the films $v^{[1]}$:

$$\frac{1}{\theta} \nabla_{yp} \cdot (\mathrm{div}_{yp}(\mathcal{M}(v^{[1]}))) = \frac{\mathcal{K}_0}{\eta} [\boldsymbol{\sigma}_f^{[0]} \cdot \boldsymbol{N}] \cdot \boldsymbol{N} - \mathrm{i}\omega\rho_p t v^{[0]} \quad \text{on } \Gamma_p, \tag{B 10}$$

$$v^{[1]} = 0 \quad \text{and} \quad \nabla_{yp} v^{[1]} \cdot \boldsymbol{n} = 0 \quad \text{on } \partial\Gamma_p. \tag{B 11a,b}$$

To solve this problem, we consider the space W_{Γ_p} composed of the complex velocities w defined in Γ_p that satisfy the boundary conditions $w = 0$ and $\nabla_{yp} w \cdot \boldsymbol{n} = 0$ on $\partial\Gamma_p$. Then, equation (B 10) is multiplied by a test function $\overline{w}$ in W_{Γ_p}. Noting that $v^{[0]} = 0$ and that the integral transformation process is similar to that performed in appendix A, the respective variational formulation is given by

$$\forall w \in W_{\Gamma_p}, \quad \frac{1}{\theta} \int_{\Gamma_p} \mathcal{N}(v^{[1]}, w)\, \mathrm{d}\Gamma = \frac{\mathcal{K}_0}{\eta} \int_{\Gamma_p} [\boldsymbol{\sigma}_f^{[0]} \cdot \boldsymbol{N}] \cdot \boldsymbol{N} \overline{w}\, \mathrm{d}\Gamma. \tag{B 12}$$

This is a linear problem forced by the stress exerted by the fluid $\boldsymbol{\sigma}_f^{[0]}$ at the leading order, which is induced by the macroscopic pressure gradient $\nabla_x p^{(0)}$ (see (B 8)–(B 9)). The solution is therefore given by

$$v^{[1]} = -\frac{\mathcal{K}_0 \theta}{\eta} \widetilde{\boldsymbol{b}}_r(y, \omega) \cdot \nabla_x p^{(0)} = -\frac{\widehat{\boldsymbol{b}}_r(y, \omega)}{\eta} \cdot \nabla_x p^{(0)}, \tag{B 13}$$

where $\widehat{\boldsymbol{b}}_r(y, \omega)$ has units of m^2 and represents the local response of the films to the stress exerted by the fluid, which is induced by the macroscopic pressure gradient. It should be noted that (i) $v^{[1]}$ is only defined on Γ_p and (ii) the frequency dependence of $\widehat{\boldsymbol{b}}_r(y, \omega)$ is due to the visco-inertial stress exerted by the fluid but not from the inertia of the films themselves.

At the next order, the fluid flow problem reads as

$$\mathrm{div}_y(\boldsymbol{\sigma}_f^{[1]}) = \mathrm{i}\omega\rho_0 \boldsymbol{v}^{[1]} \quad \text{in } \Omega_f, \tag{B 14}$$

$$\nabla_y \cdot \boldsymbol{v}^{[1]} = 0 \quad \text{in } \Omega_f, \tag{B 15}$$

$$\boldsymbol{v}^{[1]} = v^{[1]}\boldsymbol{N} \quad \text{on } \Gamma_p; \quad \boldsymbol{v}^{[1]} = \boldsymbol{0} \quad \text{on } \Gamma_s. \tag{B 16a,b}$$

Since $v^{[1]}$ is known, this set can be solved as follows. We consider the Ω-periodic unique vector $\boldsymbol{v}$ defined in Ω_f that is divergence free, $\nabla_y \cdot \boldsymbol{v} = 0$, and takes the value $\boldsymbol{v} = v^{[1]}\boldsymbol{N}$ on Γ_p and $\boldsymbol{v} = 0$ on Γ_s. Since $v^{[1]}$ is linear in the macroscopic pressure gradient, one has that $\boldsymbol{v}$ is also linear in $\nabla_x p^{(0)}$. The construction of $\boldsymbol{v}$ is performed by following the same ideas as developed in Ladyzhenskaya (1963, Ch. 1). We then set $\boldsymbol{v}^{[1]} = \boldsymbol{v} + \boldsymbol{U}$ and look for $\boldsymbol{U} \in W_r$, where W_r is the space of Darcy's velocities considering the films as perfectly rigid.

By multiplying (B 14) by $\overline{\boldsymbol{w}}$ and integrating over Ω_f, the following variational formulation is obtained after integration by parts:

$$\begin{aligned} \forall \boldsymbol{w} \in W_r, \quad & \int_{\Omega_f} 2\boldsymbol{D}_y(\boldsymbol{U}) : \boldsymbol{D}_y(\overline{\boldsymbol{w}})\, \mathrm{d}\Omega + \frac{\mathrm{i}\omega\rho_0}{\eta} \int_{\Omega_f} \boldsymbol{U} \cdot \overline{\boldsymbol{w}}\, \mathrm{d}\Omega \\ & = -\int_{\Omega_f} 2\boldsymbol{D}_y(\boldsymbol{v}) : \boldsymbol{D}_y(\overline{\boldsymbol{w}})\, \mathrm{d}\Omega - \frac{\mathrm{i}\omega\rho_0}{\eta} \int_{\Omega_f} \boldsymbol{v} \cdot \overline{\boldsymbol{w}}\, \mathrm{d}\Omega. \end{aligned} \tag{B 17}$$

The Lax–Milgram theorem applied to (B 17) ensures the existence of a unique $\boldsymbol{U}$. Since $\boldsymbol{v}$ is linear in the macroscopic pressure gradient, $\boldsymbol{U}$ is also linear in $\nabla_x p^{(0)}$. Then, the corrector $\boldsymbol{v}^{[1]}$ takes the form

$$\boldsymbol{v}^{[1]} = -\frac{\widehat{\boldsymbol{B}}_r(y, \omega)}{\eta} \cdot \nabla_x p^{(0)}, \tag{B 18}$$

where $\widehat{\boldsymbol{B}}_r$ has units of m^2 and represents the local contribution to the fluid flow generated by the vibration of the films in response to the excitation by the fluid flow at the leading order (i.e. at α^0).

Finally, the averaged velocity $\langle \boldsymbol{v}^{(0)} \rangle = \langle \boldsymbol{v}^{[0]} \rangle + \alpha \langle \boldsymbol{v}^{[1]} \rangle$ reads as

$$\langle \boldsymbol{v}^{(0)} \rangle = -\left(\frac{\boldsymbol{k}_r(\omega)}{\eta} + \frac{\mathrm{i}\omega}{\omega_e} \frac{\boldsymbol{B}_r(\omega)}{\eta} \right) \cdot \nabla_x p^{(0)}, \tag{B 19}$$

where $\boldsymbol{k}_r(\omega) = \langle \widehat{\boldsymbol{k}}_r(y, \omega) \rangle$ and $\boldsymbol{B}_r(\omega) = \langle \widehat{\boldsymbol{B}}_r(y, \omega) \rangle$. The symmetry of these two tensors is inherited from the symmetry of the form (2.34).

Now, we focus on the case where viscosity effects dominate. Hence, the term representing the inertia of the fluid in (B 1) (i.e. $\mathrm{i}\omega\rho_0 \boldsymbol{v}^{(0)}$) is negligible. Considering the viscous, elastic and forcing terms in the variational formulation (2.33), setting $\boldsymbol{w} = \boldsymbol{v}^{(0)}$ and $w = v^{(0)}$, and using (B 19), one obtains for $\omega \ll \omega_e$ and $\omega \ll \omega_{vr}$

$$\begin{aligned} & \eta \int_{\Omega_f} 2|\boldsymbol{D}_y(\boldsymbol{v}^{(0)})|^2\, \mathrm{d}\Omega - \mathrm{i}\frac{E_p I}{\omega} \int_{\Gamma_p} \mathcal{N}(v^{(0)}, v^{(0)})\, \mathrm{d}\Gamma \\ & \quad = +\Omega_f \nabla_x p^{(0)} \cdot \frac{\boldsymbol{k}_{r0}}{\eta} \cdot \nabla_x p^{(0)} - \mathrm{i}\Omega_f \frac{\omega}{\omega_e} \nabla_x p^{(0)} \cdot \frac{\boldsymbol{B}_{r0}}{\eta} \cdot \nabla_x p^{(0)}, \end{aligned} \tag{B 20}$$

where $\boldsymbol{k}_{r0} = \boldsymbol{k}_r(\omega \ll \omega_{vr})$ and $\boldsymbol{B}_{r0} = \boldsymbol{B}_r(\omega \ll \omega_{vr})$. By equating the real and imaginary parts, one directly proves that $\boldsymbol{k}_{r0}$ and $\boldsymbol{B}_{r0}$ are positive. Moreover, due to the symmetry of the form (2.34), these tensors are symmetric.

The micro–macro viscous dissipated and elastic stored power relationships are given by

$$\eta \int_{\Omega_f} 2|\boldsymbol{D}_y(\boldsymbol{v}^{(0)})|^2 \,\mathrm{d}\Omega = \Omega_f \nabla_x p^{(0)} \cdot \frac{\boldsymbol{k}_{r0}}{\eta} \cdot \nabla_x p^{(0)}, \tag{B 21}$$

$$E_p I \omega_e \int_{\Gamma_p} \mathcal{N}(u^{(0)}, u^{(0)}) \,\mathrm{d}\Gamma = \Omega_f \nabla_x p^{(0)} \cdot \frac{\boldsymbol{B}_{r0}}{\eta} \cdot \nabla_x p^{(0)}. \tag{B 22}$$

Finally, it is of interest to investigate the behaviour of the tensors $\boldsymbol{k}_{r\infty} = \mathcal{K}_{r\infty}\boldsymbol{I}$ and $\boldsymbol{B}_{r\infty} = B_{r\infty}\boldsymbol{I}$, which correspond to the values of the respective tensors when viscosity effects are negligible, i.e. for $\omega \gg \omega_{vr}$. Recalling that the inertia of the films does not contribute to the fluid flow when $\omega \ll \omega_e$, the variational formulation (2.33) evaluated at $\boldsymbol{w} = \boldsymbol{v}^{(0)}$ and divided by the volume of the pores reads as

$$\frac{\mathrm{i}\omega\rho_0}{\eta}\langle|\boldsymbol{v}^{(0)}|^2\rangle + \frac{E_p I}{\mathrm{i}\omega\eta}\frac{1}{\Omega_f}\int_{\Gamma_p} \mathcal{N}(v^{(0)}, v^{(0)}) \,\mathrm{d}\Gamma = \langle \boldsymbol{v}^{(0)}\rangle \cdot \left(\mathcal{K}_{r\infty} + \frac{\mathrm{i}\omega}{\omega_e} B_{r\infty}\right)^{-1} \cdot \langle \overline{\boldsymbol{v}}^{(0)}\rangle. \tag{B 23}$$

This equation can be rewritten using (3.6), (3.8) and (3.3) for $\rho_p = 0$ and $\omega \ll \omega_e$, i.e. $\alpha_\infty = \alpha_{\infty r}$, as

$$\frac{1}{\mathcal{K}_{r0}}\frac{\mathrm{i}\omega}{\omega_{vr}}\left(1 - \frac{\mathcal{K}_{r0}}{\mathcal{K}_0}\frac{\omega_e\omega_{vr}}{\omega^2}\right) = \frac{1}{\mathcal{K}_{r\infty}}\left(1 + \frac{\mathrm{i}\omega}{\omega_e}\frac{B_{r\infty}}{\mathcal{K}_{r\infty}}\right)^{-1}. \tag{B 24}$$

Considering that $\mathcal{K}_{r\infty} = \eta/\mathrm{i}\omega\rho_0\alpha_{\infty r} = \mathcal{K}_{r0}\omega_{vr}/\mathrm{i}\omega$, the resolution of the resulting equation yields

$$B_{r\infty} = -\mathcal{K}_{r0}\frac{\mathcal{K}_{r0}}{\mathcal{K}_0}\left(\frac{\omega_{vr}\omega_e}{\omega^2}\right)^2\left(1 - \frac{\mathcal{K}_{r0}}{\mathcal{K}_0}\frac{\omega_{vr}\omega_e}{\omega^2}\right)^{-1}. \tag{B 25}$$

Appendix C

The case of very flexible films $E_p I \to 0$ (or high frequencies $\omega \to \infty$, as will become apparent further below) is now considered. The procedure is similar to that described in appendix B. A small parameter $\beta = \omega_e/\mathrm{i}\omega \to 0$ is first identified from (B 4). The variables are looked for as expansion series of the type $\boldsymbol{v}^{(0)} = \sum_{i=0}^{\infty}\beta^i\boldsymbol{v}^{[i]}$, $\boldsymbol{\sigma}_f^{(1)} = \sum_{i=0}^{\infty}\beta^i\boldsymbol{\sigma}_f^{[i]}$ and $v^{(0)} = \sum_{i=0}^{\infty}\beta^i v^{[i]}$. At β^0, one obtains the oscillatory Stokes flow problem with boundary conditions $\boldsymbol{v}^{[0]} = 0$ on Γ_s and $\boldsymbol{v}^{[0]} = v^{[0]}\boldsymbol{N}$ on Γ_p, together with the following condition on the films:

$$[\boldsymbol{\sigma}_f^{[0]} \cdot \boldsymbol{N}] \cdot \boldsymbol{N} = \mathrm{i}\omega\rho_p t v^{[0]} \quad \text{on } \Gamma_p, \tag{C 1}$$

and clamping boundary conditions $v^{[0]} = 0$ and $\nabla_{yp} v^{[0]} \cdot \boldsymbol{n} = 0$ on $\partial\Gamma_p$. The variational formulation associated with this problem is given by

$$\forall \boldsymbol{w} \in \mathcal{W}, \quad \mathcal{K}_0 \int_{\Omega_f} 2\boldsymbol{D}_y(\boldsymbol{v}^{[0]}) : \boldsymbol{D}_y(\overline{\boldsymbol{w}}) \,\mathrm{d}\Omega + \frac{\mathrm{i}\omega}{\omega_v}\frac{1}{\alpha_{\infty\varrho}}\int_{\Omega_f\cup\Gamma_p} \widetilde{\rho}\boldsymbol{v}^{[0]} \cdot \overline{\boldsymbol{w}} \,\mathrm{d}\Omega$$
$$= -\frac{\mathcal{K}_0}{\eta}\nabla_x p^{(0)} \cdot \int_{\Omega_f} \overline{\boldsymbol{w}} \,\mathrm{d}\Omega. \tag{C 2}$$

Therefore, the solution of the problem reads as

$$\boldsymbol{v}^{[0]} = -\frac{\widehat{\boldsymbol{k}}_s(y,\omega)}{\eta}\cdot\boldsymbol{\nabla}_x p^{(0)}. \tag{C 3}$$

It must be emphasised that, even though the variational formulation and the solution of the problem resemble the classical dynamic Darcy's law set in the pore space, the local fluid velocity field is different from that in the case where the films are absent. This is because (i) a condition of normal fluid flow is imposed on the film surface and (ii) the global inertia is determined by the distribution of density of the fluid–film system, which is accounted for by $\widetilde{\rho}$, instead of the fluid density alone.

The problem governing the corrector $\boldsymbol{v}^{[1]}$ corresponds to an oscillatory Stokes problem without macroscopic pressure gradient. In addition, the boundary conditions $\boldsymbol{v}^{[1]} = 0$ on Γ_s and $\boldsymbol{v}^{[1]} = v^{[1]}\boldsymbol{N}$ on Γ_p are considered, together with the following condition on the films:

$$\mathrm{i}\omega\rho_p t v^{[1]} + [\boldsymbol{\sigma}_f^{[1]}\cdot\boldsymbol{N}]\cdot\boldsymbol{N} = -\frac{\eta}{\mathcal{K}_0\theta}\boldsymbol{\nabla}_{yp}\cdot(\mathrm{div}_{yp}(\mathcal{M}(v^{[0]}))) \quad \text{on } \Gamma_p. \tag{C 4}$$

This equation indicates that the equilibrium of the films, for which the motion is imposed by the fluid flow at the leading order (i.e. at β^0), is realised by the velocity field at the next order $\boldsymbol{v}^{[1]}$.

The variational formulation associated with this problem is given by

$$\begin{aligned}\forall \boldsymbol{w}\in\mathcal{W},\quad & \mathcal{K}_0\int_{\Omega_f} 2\boldsymbol{D}_y(\boldsymbol{v}^{[1]}) : \boldsymbol{D}_y(\overline{\boldsymbol{w}})\,\mathrm{d}\Omega + \frac{\mathrm{i}\omega}{\omega_v}\frac{1}{\alpha_\infty\varrho}\int_{\Omega_f\cup\Gamma_p}\widetilde{\rho}\boldsymbol{v}^{[1]}\cdot\overline{\boldsymbol{w}}\,\mathrm{d}\Omega \\ &= -\frac{1}{\theta}\int_{\Gamma_p}\mathcal{N}(v^{[0]},\boldsymbol{w})\,\mathrm{d}\Gamma.\end{aligned} \tag{C 5}$$

Noting that the forcing term is related to the balance of $v^{[0]}$ and the film velocity is linear in the macroscopic pressure gradient, the solution of the problem is written in close analogy with Darcy's law as

$$\boldsymbol{v}^{[1]} = +\frac{\widehat{\boldsymbol{B}}_s(y,\omega)}{\eta}\cdot\boldsymbol{\nabla}_x p^{(0)}. \tag{C 6}$$

The term $\widehat{\boldsymbol{B}}_s(y,\omega)$ has units of m^2 and determines the local additional flow required to equilibrate the films which are undergoing deformation imposed by the flow at the leading order (at β^0). Then, the averaged velocity $\langle\boldsymbol{v}^{(0)}\rangle = \langle\boldsymbol{v}^{[0]}\rangle + \beta\langle\boldsymbol{v}^{[1]}\rangle$ reads as

$$\langle\boldsymbol{v}^{(0)}\rangle = -\left(\frac{\boldsymbol{k}_s(\omega)}{\eta} - \frac{\omega_e}{\mathrm{i}\omega}\frac{\boldsymbol{B}_s(\omega)}{\eta}\right)\cdot\boldsymbol{\nabla}_x p^{(0)}. \tag{C 7}$$

This expression holds as long as $\beta = \omega_e/\mathrm{i}\omega \to 0$. Such a condition cannot be satisfied at very low frequencies. In such a case, the results presented in appendix B should be considered. This means that the films behave as quasi-rigid at low frequencies. Despite this, there could exist a material for which $\omega_e \ll \omega \ll \omega_{vs}$. Provided that this condition is satisfied, one can consider the viscous, elastic and forcing terms in the variational

formulation (2.33), set $\boldsymbol{w} = \boldsymbol{v}^{(0)}$ and $w = v^{(0)}$, and use (C 7) to obtain

$$\eta \int_{\Omega_f} 2|\boldsymbol{D}_y(\boldsymbol{v}^{(0)})|^2 \,\mathrm{d}\Omega + \frac{E_p I}{\mathrm{i}\omega} \int_{\Gamma_p} \mathcal{N}(v^{(0)}, v^{(0)}) \,\mathrm{d}\Gamma$$
$$= +\Omega_f \nabla_x p^{(0)} \cdot \frac{\boldsymbol{k}_{s0}}{\eta} \cdot \nabla_x p^{(0)} + \Omega_f \frac{\omega_e}{\mathrm{i}\omega} \nabla_x p^{(0)} \cdot \frac{\boldsymbol{B}_{s0}}{\eta} \cdot \nabla_x p^{(0)}, \tag{C 8}$$

where $\boldsymbol{k}_{s0}$ and $\boldsymbol{B}_{s0}$ are the viscous permeability and elasticity-induced corrector for very flexible films in the absence of inertial effects. One may infer that $\boldsymbol{k}_{s0}$ can be reasonably estimated by the static viscous permeability of the pore space without films.

By equating the real and imaginary parts in (C 8), one directly proves that both tensors are positive, while their symmetry is ensured by that of the form (2.34). Furthermore, the micro–macro viscous dissipated and elastic stored power relationships are given by

$$\eta \int_{\Omega_f} 2|\boldsymbol{D}_y(\boldsymbol{v}^{(0)})|^2 \,\mathrm{d}\Omega = \Omega_f \nabla_x p^{(0)} \cdot \frac{\boldsymbol{k}_{s0}}{\eta} \cdot \nabla_x p^{(0)}, \tag{C 9}$$

$$\frac{E_p I \omega^2}{\omega_e} \int_{\Gamma_p} \mathcal{N}(u^{(0)}, u^{(0)}) \,\mathrm{d}\Gamma = \Omega_f \nabla_x p^{(0)} \cdot \frac{\boldsymbol{B}_{s0}}{\eta} \cdot \nabla_x p^{(0)}. \tag{C 10}$$

Finally, it is of interest to investigate the behaviour of $\boldsymbol{k}_s$ and $\boldsymbol{B}_s$ when $\omega \gg \omega_{vs}$. To do so, the variational formulation (2.33) is evaluated at $\boldsymbol{w} = \boldsymbol{v}^{(0)}$, divided by Ω_f, and the viscous term is omitted, i.e.

$$\frac{\mathrm{i}\omega\rho_0}{\eta} \left(\langle |\boldsymbol{v}^{(0)}|^2 \rangle + \frac{\rho_p}{\rho_0} \frac{t}{\Omega_f} \int_{\Gamma_p} |v^{(0)}|^2 \,\mathrm{d}\Gamma \right) + \frac{E_p I}{\mathrm{i}\omega\eta} \frac{1}{\Omega_f} \int_{\Gamma_p} \mathcal{N}(v^{(0)}, v^{(0)}) \,\mathrm{d}\Gamma$$
$$= \langle \boldsymbol{v}^{(0)} \rangle \cdot \left(\mathcal{K}_{s\infty} - \frac{\omega_e}{\mathrm{i}\omega} B_{s\infty} \right)^{-1} \cdot \langle \overline{\boldsymbol{v}}^{(0)} \rangle. \tag{C 11}$$

Noting that $\mathcal{K}_{s\infty} = \mathcal{K}_s(\omega \gg \omega_{vs}) = \mathcal{K}_{s0}\omega_{vs}/\mathrm{i}\omega$ and using (3.6), (3.3), (3.4) and (3.8), one can rewrite this expression as

$$\left(\mathcal{K}_{s0} \frac{\omega_{vs}}{\mathrm{i}\omega} - \frac{\omega_e}{\mathrm{i}\omega} B_{s\infty} \right) \frac{1}{\mathcal{K}_0} \left(\frac{\mathrm{i}\omega}{\omega_v} + \frac{\omega_e}{\mathrm{i}\omega} \frac{\theta_g}{\theta} \right) = 1, \tag{C 12}$$

which leads to

$$B_{s\infty} = \mathcal{K}_{s0} \frac{\omega_{vs}}{\omega_e} \frac{1}{1 - \dfrac{\omega^2}{\omega_g^2}}. \tag{C 13}$$

REFERENCES

ALLARD, J. F. & ATALLA, N. 2009 *Propagation of Sound in Porous Media: Modeling Sound Absorbing Materials*. Wiley.

AURIAULT, J. L., BORNE, L. & CHAMBON, R. 1985 Dynamics of porous saturated media, checking of the generalized law of Darcy. *J. Acoust. Soc. Am.* **77** (5), 1641–1650.

AURIAULT, J. L., BOUTIN, C. & GEINDREAU, C. 2009 *Homogenization of Coupled Phenomena in Heterogeneous Media*. ISTE Ltd and Wiley.

BIOT, M. A. 1956*a* Theory of propagation of elastic waves in a fluid-saturated porous solid. I. Low-frequency range. *J. Acoust. Soc. Am.* **28**, 168–178.

BIOT, M. A. 1956*b* Theory of propagation of elastic waves in a fluid-saturated porous solid. II. Higher frequency range. *J. Acoust. Soc. Am.* **28**, 179–191.

BOLTON, J. S. 2013 The modeling of unconventional sound absorbing materials: microperforated films and closed cell foams. In *One-Day International Conference, Lightweighting and Acoustical Materials in Vehicles. Université de Technologie de Compiègne – 22 October 2014, Compiègne, France*.

BONGARD, F., LISSEK, H. & MOSIG, J. R. 2010 Acoustic transmission line metamaterial with negative/zero/positive refractive index. *Phys. Rev.* B **82**, 094306.

BOUTIN, C. 2013 Acoustics of porous media with inner resonators. *J. Acoust. Soc. Am.* **134** (6), 4717–4729.

BOUTIN, C. & AURIAULT, J. L. 1990 Dynamic behaviour of porous media saturated by a viscoelastic fluid. Application to bituminous concretes. *Intl J. Engng Sci.* **28** (11), 1157–1181.

BOUTIN, C., ROYER, P. & AURIAULT, J. L. 1998 Acoustic absorption of porous surfacing with dual porosity. *Intl J. Solids Struct.* **35**, 4709–4737.

BRAVO, T., MAUDRY, C. & PINHÈDE, C. 2012 Vibroacoustic properties of thin micro-perforated panel absorbers. *J. Acoust. Soc. Am.* **132** (2), 789–798.

BROWN, D. L., POPOV, P. & EFENDIEV, Y. 2011 On homogenization of Stokes flow in slowly varying media with applications to fluid–structure interaction. *Int. J. Geomath.* **2**, 281–305.

BROWN, D. L., POPOV, P. & EFENDIEV, Y. 2014 Effective equations for fluid–structure interaction with applications to poroelasticity. *Appl. Anal.* **4**, 771–790.

COMSOL 2013 Comsol Multiphysics documentation version 4.3b.

CUMMER, S. A., CHRISTENSEN, J. & ALÙ, A. 2016 Controlling sound with acoustic metamaterials. *Nav. Rev. Mater.* **1**, 16001.

DAILEY, H. L., YALCIN, H. C. & GHADIALI, S. N. 2007 Fluid–structure modeling of flow-induced alveolar epithelial cell deformation. *Comput. Struct.* **85**, 1066–1071.

FILIPPI, P. J. T. 2008 *Vibrations and Acoustic Radiation of Thin Structures*. ISTE Ltd and Wiley.

GRIFFITHS, S., NENNIG, B. & JOB, S. 2017 Porogranular materials composed of elastic Helmholtz resonators for acoustic wave absorption. *J. Acoust. Soc. Am.* **141** (1), 254–264.

GROBY, J.-P., LAGARRIGUE, C., BROUARD, B., DAZEL, O., TOURNAT, V. & NENNIG, B. 2015 Enhancing the absorption properties of acoustic porous plates by periodically embedding Helmholtz resonators. *J. Acoust. Soc. Am.* **137** (1), 273–280.

HABAULT, D. 1999 *Fluid–Structure Interactions in Acoustics*. Springer.

ISO 10534-2:2001 2001 Acoustics – Determination of sound absorption coefficient and impedance in impedance tubes – Part 2: Transfer-function method. Standard. International Organization for Standardization, Geneva, CH.

JOHNSON, D. L., KOPLIK, J. & DASHEN, R. 1987 Theory of dynamic permeability and tortuosity in fluid-saturated porous media. *J. Fluid Mech.* **176**, 379–402.

KRYNKIN, A., UMNOVA, O., BOON CHONG, A. Y., TAHERZADEH, S. & ATTENBOROUGH, K. 2010 Predictions and measurements of sound transmission through a periodic array of elastic shells in air. *J. Acoust. Soc. Am.* **128** (6), 3496–3506.

LADYZHENSKAYA, O. 1963 *The Mathematical Theory of Viscous Incompressible Flow*. Gordon and Breach Science Publishers.

LAFARGE, D., LEMARINIER, P., ALLARD, J. F. & TARNOW, V. 1997 Dynamic compressibility of air in porous structures at audible frequencies. *J. Acoust. Soc. Am.* **102** (4), 1995–2006.

LAFARGE, D. & NEMATI, N. 2013 Nonlocal Maxwellian theory of sound propagation in fluid-saturated rigid-framed porous media. *Wave Motion* **50** (6), 1016–1035.

LEBENTAL, B. & BOURQUIN, F. 2012 Visco-acoustic modelling of a vibrating plate interacting with water confined in a domain of micrometric size. *J. Sound Vib.* **331** (8), 1870–1886.

LECLAIRE, P., UMNOVA, O., DUPONT, T. & PANNETON, R. 2015 Acoustical properties of air-saturated porous material with periodically distributed dead-end pores. *J. Acoust. Soc. Am.* **137** (4), 1772–1782.

LEE, C. K. & MEI, C. C. 1997 Re-examination of the equations of poroelasticity. *Intl J. Engng Sci.* **35**, 329–352.

LEE, Y. Y., LEE, E. W. M. & NG, C. F. 2005 Sound absorption of a finite flexible micro-perforated panel backed by an air cavity. *J. Sound Vib.* **287**, 227–243.

LEROY, S. & CHARLAIX, E. 2011 Hydrodynamic interactions for the measurement of thin film elastic properties. *J. Fluid Mech.* **674**, 389–407.

LI, C., CAZZOLATO, B. & ZANDER, A. 2016 Acoustic impedance of micro perforated membranes: velocity continuity condition at the perforation boundary. *J. Acoust. Soc. Am.* **139** (1), 93–103.

LÓPEZ DE HARO, M., DEL RÍO, J. A. P. & WHITAKER, S. 1996 Flow of Maxwell fluids in porous media. *Trans. Porous Med.* **25** (2), 167–192.

LOVE, A. E. H. 1888 On the small free vibrations and deformations of elastic shells. *Phil. Trans. R. Soc. Lond.* A **179**, 491–549.

MA, G. & SHENG, P. 2016 Acoustic metamaterials: from local resonances to broad horizons. *Sci. Adv.* **2** (2), e1501595.

NORRIS, A. N. & WICKHAM, G. 1993 Elastic Helmholtz resonators. *J. Acoust. Soc. Am.* **93**, 617–630.

OLNY, X. & BOUTIN, C. 2003 Acoustic wave propagation in double porosity media. *J. Acoust. Soc. Am.* **113** (6), 73–89.

PANASENKO, G. P. & STAVRE, R. 2012 Asymptotic analysis of a viscous fluid–thin plate interaction: periodic flow. *C. R. Méc.* **340**, 590–595.

PRIDE, S. R., MORGAN, F. D. & GANGI, A. F. 1993 Drag forces of porous-medium acoustics. *Phys. Rev.* B **47**, 4964–4978.

RUBENSTEIN, D. A., YIN, W. & FRAME, M. D. 2015 *Biofluid Mechanics*, 2nd edn. Academic.

SANCHEZ-PALENCIA, E. 1980 *Non-Homogeneous Media and Vibration Theory*. Springer.

SMEULDERS, D. M. J., EGGELS, R. L. G. M. & VAN DONGEN, M. E. H. 1992 Dynamic permeability: reformulation of theory and new experimental and numerical data. *J. Fluid Mech.* **245**, 211–227.

VENEGAS, R. & BOUTIN, C. 2017 Acoustics of sorptive porous materials. *Wave Motion* **68**, 162–181.

VENEGAS, R. & UMNOVA, O. 2011 Acoustical properties of double porosity granular materials. *J. Acoust. Soc. Am.* **130** (5), 2765–2776.

YANG, Z., MEI, J., YANG, M., CHAN, N. & SHENG, P. 2008 Membrane-type acoustic metamaterial with negative dynamic mass. *Phys. Rev. Lett.* **101**, 204301.